2024-03-26

Discovery of SQSTM1/p62-dependent P-bodies that regulate the NLRP3 inflammasome

Barrow, ER

10.1016/j.celrep.2024.113935
Cell Reports
Elsevier BV

Cell Reports

Article

Discovery of SQSTM1/p62-dependent P-bodies that regulate the NLRP3 inflammasome

Graphical abstract

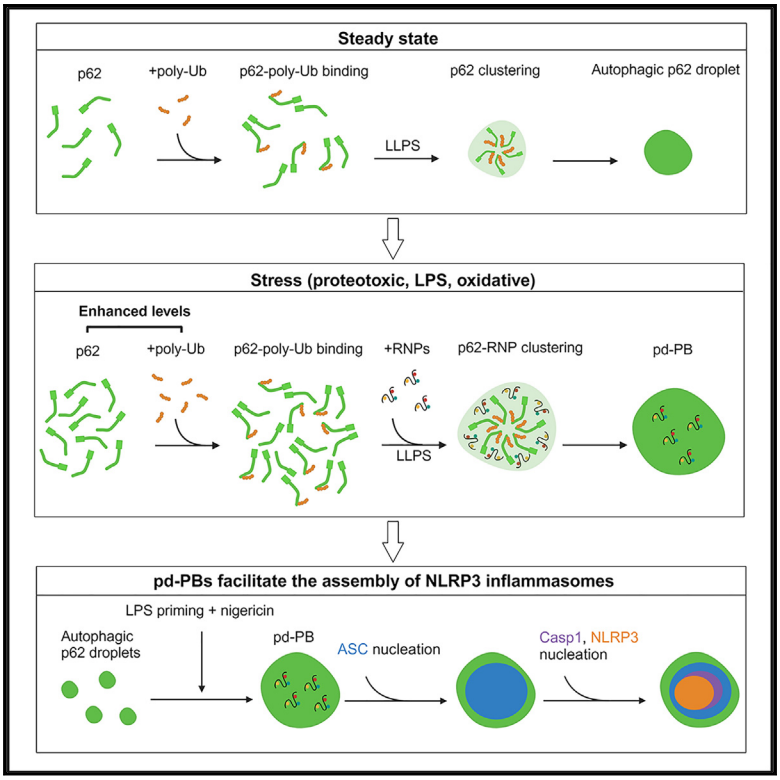

Highlights

- p62 droplets are transformed to a type of P-bodies, pd-PBs, under stress conditions
- p62 droplet formation drives the nucleation of pd-PBs
- pd-PBs serve as platforms to regulate the formation of NLRP3 inflammasomes
- pd-PBs promote NLRP3 inflammasome activation

Authors

Elizabeth R. Barrow, Evelina Valionyte, Chris R. Baxter, ..., Vikram Sharma, Boxun Lu, Shouqing Luo

Correspondence

luboxun@fudan.edu.cn (B.L.), shouqing.luo@plymouth.ac.uk (S.L.)

In brief

Barrow et al. demonstrate that stress conditions convert autophagic p62 droplets to a type of enlarged P-bodies, p62-dependent P-bodies (pd-PBs), via enhanced p62 condensation. pd-PBs recruit the NLRP3 inflammasome adaptor ASC to assemble the NLRP3 inflammasome and induce inflammation-associated cytotoxicity.

Barrow et al., 2024, Cell Reports *43*, 113935
March 26, 2024
https://doi.org/10.1016/j.celrep.2024.113935

CellPress

Cell Reports

CellPress
OPEN ACCESS

Article

Discovery of SQSTM1/p62-dependent P-bodies that regulate the NLRP3 inflammasome

Elizabeth R. Barrow,[1,5] Evelina Valionyte,[1,5] Chris R. Baxter,[1] Yi Yang,[1] Sharon Herath,[1] William A. O'Connell,[1] Justyna Lopatecka,[2] Alexander Strachan,[3] Waldemar Woznica,[1] Holly N. Stephenson,[1] Gyorgy Fejer,[2] Vikram Sharma,[2] Boxun Lu,[4,*] and Shouqing Luo[1,6,*]

[1]Peninsula Medical School, Faculty of Health, University of Plymouth, Research Way, PL6 8BU Plymouth, UK
[2]School of Biomedical Sciences, Faculty of Health, University of Plymouth, Drake Circus, PL4 8AA Plymouth, UK
[3]Plymouth Electron Microscopy Centre, University of Plymouth, Drake Circus, PL4 8AA Plymouth, UK
[4]State Key Laboratory of Medical Neurobiology, School of Life Sciences, Fudan University, Shanghai 200438, China
[5]These authors contributed equally
[6]Lead contact
*Correspondence: luboxun@fudan.edu.cn (B.L.), shouqing.luo@plymouth.ac.uk (S.L.)
https://doi.org/10.1016/j.celrep.2024.113935

SUMMARY

Autophagy and ribonucleoprotein granules, such as P-bodies (PBs) and stress granules, represent vital stress responses to maintain cellular homeostasis. SQSTM1/p62 phase-separated droplets are known to play critical roles in selective autophagy; however, it is unknown whether p62 can exist as another form in addition to its autophagic droplets. Here, we found that, under stress conditions, including proteotoxicity, endotoxicity, and oxidation, autophagic p62 droplets are transformed to a type of enlarged PBs, termed p62-dependent P-bodies (pd-PBs). p62 phase separation is essential for the nucleation of pd-PBs. Mechanistically, pd-PBs are triggered by enhanced p62 droplet formation upon stress stimulation through the interactions between p62 and DDX6, a DEAD-box ATPase. Functionally, pd-PBs recruit the NLRP3 inflammasome adaptor ASC to assemble the NLRP3 inflammasome and induce inflammation-associated cytotoxicity. Our study shows that p62 droplet-to-PB transformation acts as a stress response to activate the NLRP3 inflammasome process, suggesting that persistent pd-PBs lead to NLRP3-dependent inflammation toxicity.

INTRODUCTION

Macroautophagy (referred to as autophagy) is a lysosomal degradation system mediating the clearance of aberrant cytoplasmic constituents. SQSTM1/p62 is known as an autophagy receptor critical for selective autophagic removal of substrates.[1] p62 is subject to liquid-liquid phase separation (LLPS) for its droplet formation, which is driven by the binding of polyubiquitin chains on polyubiquitinated proteins[2,3] and its chaperone protein DAXX.[4] This process is critical for its subsequent function in recruiting cargo for autophagic clearance. To date, it is unknown whether p62 can exist as another form in addition to its autophagic droplets.

Similar to p62 droplets, ribonucleoprotein (RNP) granules are a group of dynamic membrane-less biomolecular assemblies of RNAs and RNA binding proteins (RBPs), such as P-bodies (PBs), stress granules (SGs), Cajal bodies, and nuclear speckles.[5,6] RNP granules form under stress conditions when translation initiation is limited.[7,8] RNP granule condensation is governed by LLPS, depending on RNA-RNA, protein-protein, or protein-RNA interactions.[9] The intrinsically disordered regions (IDRs), oligomerization domains, and RNA-binding domains in RBPs are vital to drive the LLPS process of RNP granules.[10,11] RNP granules represent stress response machineries induced by a repertoire of stresses and are speculated to repress global protein translation[7,12] but allow the synthesis of housekeeping proteins vital for cell survival.[11] SGs and PBs are discrete RNP granules, although they share some properties and RBPs. PBs, marked by EDC4, Dcp1a, DDX6, and LSM14A, are suggested to regulate RNA degradation[13,14] and translational elongation inhibition,[7,8,15] while SGs with G3BP1, G3BP2, and Caprin-1 are involved in mRNA storage and arrest of translation initiation.[16,17] SGs are only formed by stress induction, whereas both constitutive PBs and stress-induced PBs can exist under basal and stress conditions.[18,19] The mechanisms underlying the assembly (including the establishment and maintenance) of PBs and SGs remain poorly understood. TIA1,[20] G3BP1 and G3BP2,[17,21] PRRC2C, CSDE1,[22] and UBAP2L[23] are essential for the assembly of SGs, and ubiquitination of G3BP1 is required for the disassembly of SGs.[24] However, the molecular basis for the assembly of PBs has yet to be elucidated.

Neurodegenerative diseases, such as amyotrophic lateral sclerosis (ALS) and frontotemporal lobar degeneration (FTLD), are associated with persistent RNP granules,[6,25] and mutations in RBPs such as TDP43, FUS, EWSR1, TAF15, and hnRNPA1 predispose to these diseases.[26–31] Such mutations may enhance the self-association of the low-complexity domain and stabilize the structure of RNP granules.[32] We have shown recently that

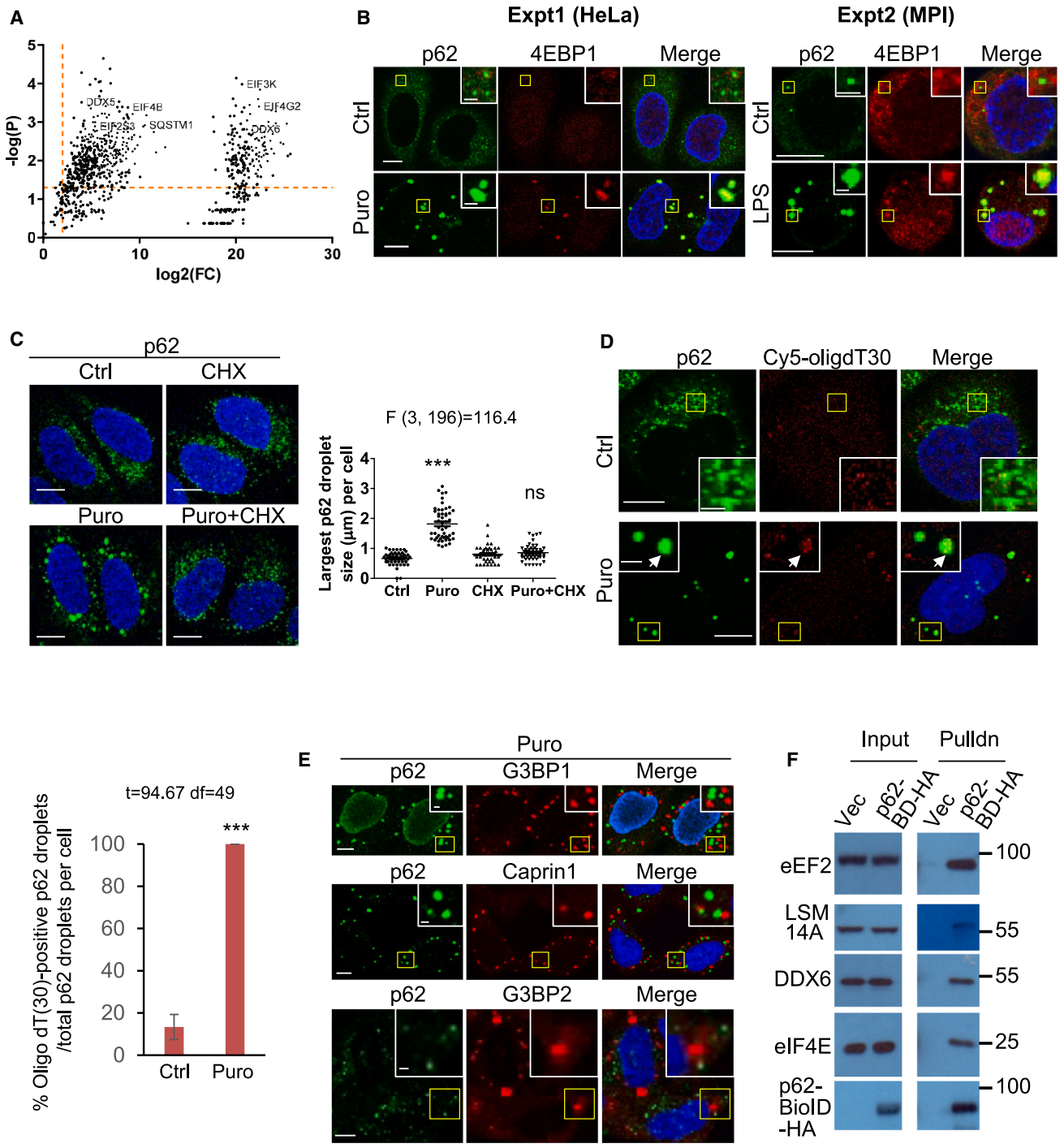

Figure 1. Identification of puromycin-enlarged p62 droplets as RNP granules

(A) The volcano plot shows significant differences and fold changes (FCs) of p62 BioID2 pull-down protein candidates over vector control-yielded non-specific ones. A few examples of mRNA-binding protein hits are shown.

(B) HeLa cells treated with control (Ctrl) or puromycin (Puro) in experiment 1 (Expt1) or primary resident macrophages (MPI cells) treated with Ctrl or lipopolysaccharide (LPS) in experiment 2 (Expt2) were co-stained for p62/4EBP1. Note that all p62/4EBP1 droplets are colocalized in cells treated with Puro.

(C) HeLa cells were treated with cycloheximide (CHX; 50 μg/mL) and/or Puro for 3.5 h. The cells were stained for p62. The size of the largest p62 droplet per cell was quantified. n = 50 cells. Data are shown as mean ± SEM. Statistical analysis was performed by one-way ANOVA with Bonferroni multiple-comparisons test.

(D) HeLa cells treated with Ctrl or Puro were subject to fluorescence *in situ* hybridization (FISH) with oligo(dT)30 and subsequently stained with anti-p62. Confocal images were acquired. White arrows denote an enlarged p62 droplet. The percentage of colocalized p62 droplets versus total p62 droplets per cell was quantified. n = 50 cells. Data are shown as mean ± SEM. Statistical analysis was performed by two-tailed unpaired t test.

(legend continued on next page)

gelation of CAG RNA repeats represses protein translation.[33] CAG RNA repeats could involve the dynamics of RNP granules. Persistent PBs and SGs are believed to nucleate protein aggregation by acting as nidi.[6] Enigmatically, a vast majority of p62 mutations are also associated with the ALS-FTLD spectrum.[34]

Here, we found that p62 droplets are transformed to a type of PBs under endotoxicity, proteotoxicity, or oxidative stress. Inflammasomes are large multiprotein fibril platforms that sense a variety of microbial and environmental stressors. Nucleation of the death fold-containing protein apoptosis-associated speck-like protein containing a CARD (ASC) is required for the assembly of inflammasomes.[35,36] p62 droplet-transformed PBs recruit the critical inflammasome adaptor ASC to drive the formation of NLR family pyrin domain containing 3 (NLRP3) inflammasomes and inflammation-associated cytotoxicity. Our study underlines p62 droplet-to-PB transformation as a stress response to activate NLRP3 inflammasomes, suggesting that persistent p62-dependent PBs (pd-PBs) may cause NLRP3-dependent inflammation toxicity.

RESULTS

Proteotoxic stress induces the formation of p62 RNP condensates independent of SGs

We initially observed that endotoxin lipopolysaccharide (LPS) significantly enhanced p62 droplet size in primary resident MPI macrophages (Figure S1A). Similarly, puromycin, among several stressors, significantly enhanced p62 droplet size (Figure S1B). Puromycin, as a natural toxin, induces the premature release of polypeptide chains from ribosomes, blocking protein synthesis and resulting in proteotoxicity.[37,38] The p62 droplets under basal (steady-state) conditions displayed a differential biophysical characteristic to the p62 droplets formed under puromycin stress, as shown by fluorescence recovery after photobleaching (FRAP). The enlarged p62 droplets, induced by puromycin, were more labile than those under basal conditions (Figure S1C; Videos S1 and S2), suggesting that the composition of puromycin-induced p62 droplets would be different from that of the p62 droplets under basal conditions.

To explore the components of the highly dynamic enlarged p62 droplets, we employed the BioID2 approach to identify p62 proximity proteins. The protein candidates were enriched in several pathways, including mRNA processing, PBs, and SGs (Figure S1D). Notably, RBPs, including eIF4E, eEF2, DDX6, and LSM14A, were enriched among the identified proteins (Figure 1A; Table S1). We noted that puromycin, which inhibits protein synthesis,[37] induced the formation of both PBs and SGs (Figure S1E). The puncta of eIF4E, which, as an RBP, localized on both SGs and PBs,[39] partially colocalized with p62 droplets in cells treated with puromycin (Figure S1F). Interestingly, Danieli et al.[40] reported that p62 condensates sequester the translation initiation factors eIF2a and eIF4E. By contrast, the eIF4E-binding protein (4EBP1) entirely colocalized with p62 droplets under puromycin treatment (Figure 1B, left). Given that puromycin may increase global protein polyubiquitination,[38] we interrogated whether the full recruitment of 4EBP1 or partial recruitment of eIF4E by p62 droplets under puromycin treatment was simply due to p62's promiscuous binding to the polyubiquitin chains on polyubiquitinated 4EBP1 or eIF4E, whose levels are likely increased by puromycin treatment. Therefore, we tested several non-RBPs, including the mammalian target of rapamycin (mTOR), transcription factor EB (TFEB), or LIMP2, and an RBP, YTHDF3. Negligible colocalization of the non-RBPs with p62 droplets was found in the cells under puromycin treatment, while there was low colocalization of YTHDF3 with p62 (Figure S1G). We reason that, generally, the amount of a certain specific polyubiquitinated protein sequestered into p62 droplets is limited, although p62 is known to recruit overall polyubiquitinated proteins.[40] On the other hand, LPS endotoxicity, which did not significantly enhance global protein polyubiquitination (Figure S1H), similarly induced the full recruitment of 4EBP1 by p62 droplets in macrophages (Figure 1B, right). Therefore, the recruitment of 4EBP1 or eIF4E by p62 droplets under stress is selective rather than promiscuous. We thus ruled out the possibility that the full recruitment of 4EBP1 by p62 droplets was due to p62 promiscuously binding to globally polyubiquitinated proteins. We speculated that stress-enlarged p62 droplets could correlate with a certain type of RNP granules. Cycloheximide (CHX) stabilizes polysomes and disrupts the mRNA-ribosome equilibrium, leading to the disassembly of cytoplasmic RNA granules such as SGs and PBs.[41,42] CHX treatment entirely abrogated the enlargement of p62 droplets by puromycin stress (Figure 1C), indicating that mRNA could be a constituent of proteotoxic stress-enlarged p62 droplets. Indeed, under puromycin treatment, enlarged p62 droplets were positive for mRNAs, as probed with 30 tandem deoxythymidines (dT) (oligo(dT)30) that complement the mRNA poly(A) tail (Figure 1D). This further suggests that stress-induced p62 droplets represent a type of RNP granules. However, puromycin-enlarged p62 droplets did not colocalize with SGs marked with G3BP1, Caprin-1, or G3BP2 (Figure 1E). Thus, proteotoxic stress-induced p62 droplets as RNP granules were independent of SGs. We confirmed that several RBPs interacted with p62 in the BioID2 assay by immunoblotting and that p62 was in proximity with LSM14A and DDX6, two specific markers of PBs (Figure 1F).

Autophagic p62 droplets are transformed into PBs under proteotoxic, endotoxic, or oxidative stress

We examined whether proteotoxicity-enlarged p62 droplets correlated with PBs. Puromycin-induced p62 droplets were found to wholly overlap with the markers of PBs, including Dcp1a (Figure S2A), DDX6, LSM14A, and EDC4 (Figures 2A–2C). We confirmed the entire colocalization of overexpressed GFP-DDX6 and HA-p62 under puromycin treatment (Figure S2B). Of note, DDX6, LSM14A, and Dcp1a did not colocalize with p62 droplets under basal conditions, but they were transformed to entirely

(C and D) The F/degree of freedom/post hoc p values are indicated. ***$p < 0.0001$.
(E) p62 droplets do not colocalize with SGs. HeLa cells treated with Puro were co-stained for p62/G3BP1 (top), p62/Caprin 1(center), or p62/G3BP2 (bottom). Images were acquired by confocal microscopy. The areas boxed in yellow are magnified.
(B–E) Scale bars, 10 μm and 2 μm (insets).
(F) Immunoblot validating several RBPs identified by p62 BioID2-HA (p62-BD-HA) pull-down.

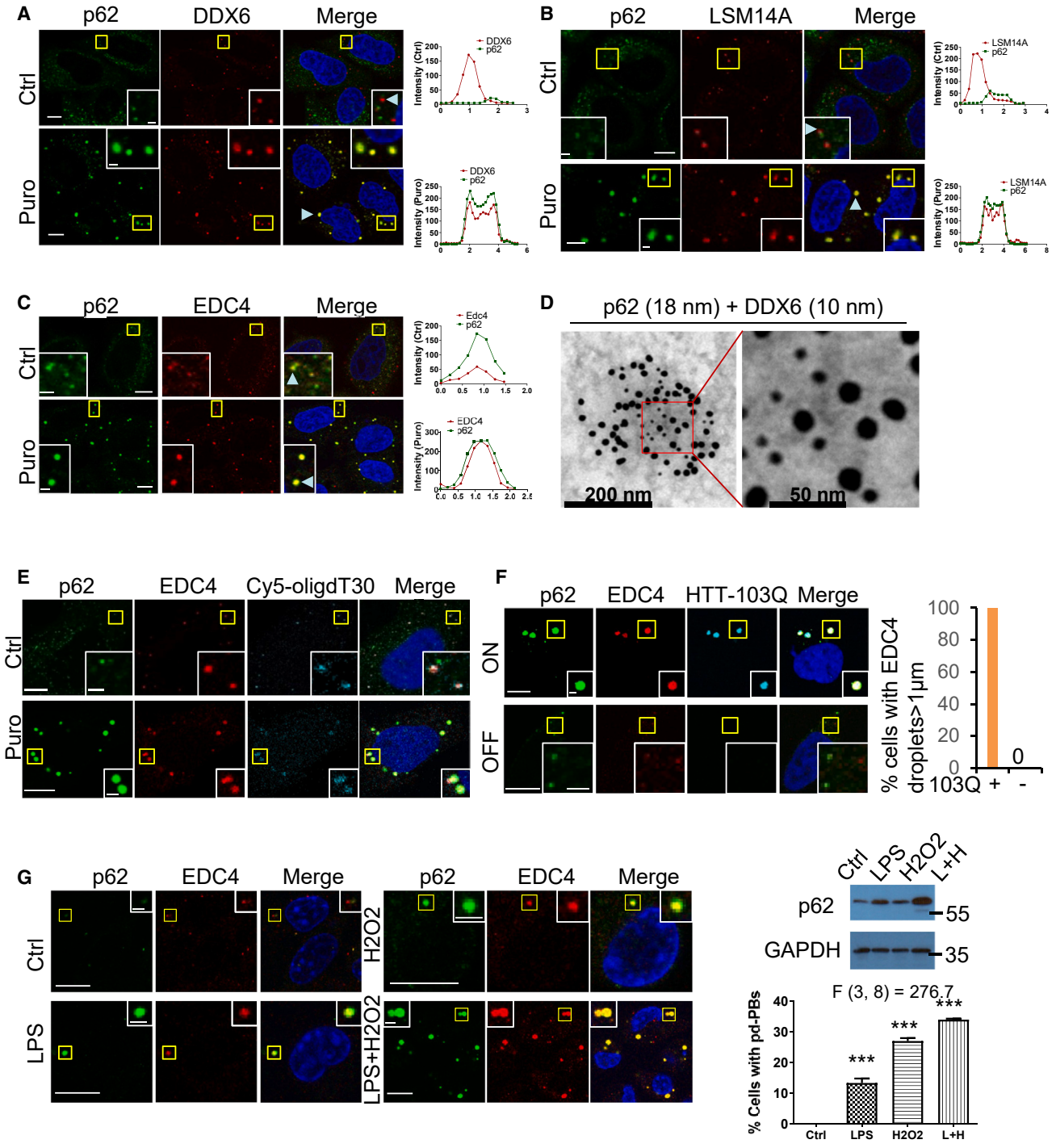

Figure 2. Proteotoxicity-enlarged p62 droplets represent p62-associated PBs

(A–C) HeLa cells treated with Ctrl or Puro were co-stained for p62/DDX6 (A), p62/LSM14A (B), or p62/EDC4 (C). Confocal images are shown. The colocalization in the droplet (annotated by the arrowhead) was quantified by line profiling.

(D) Immunogold EM. Ultra-thin sections of HeLa cells expressing Myc-p62 and HA-DDX6, treated with Puro, were stained with rabbit anti-Myc and mouse anti-HA antibodies and subsequently incubated with an anti-rabbit secondary antibody conjugated with 18-nm colloidal gold and an anti-mouse secondary antibody conjugated with 10-nm gold. Scale bars, 200 nm and 50 nm (magnification).

(E) HeLa cells treated with Ctrl or Puro were subject to FISH with oligo(dT)30 and then co-stained for p62/EDC4. Confocal images were acquired.

(F) HeLa cells with (ON) or without (OFF) induced expression of stably inducible cyan fluorescent protein (CFP)-huntingtin (HTT) exon 1-103Q (CFP-103Q), were stained for p62/EDC4. HTT-103Q forms protein aggregates. Confocal images are shown. The percentage of cells (positive or negative for CFP-103Q aggregates)

(legend continued on next page)

overlap with puromycin-induced p62 droplets (Figures 2A, 2B, S2A, and S2B). EDC4 partially colocalized with p62 droplets under basal conditions, while puromycin treatment radically enhanced the recruitment of EDC4 into p62 droplets (Figure 2C). This suggests that these RBPs could enter p62 droplets in a sequential order or potentially in a hierarchical manner, implying that, unlike other PB RBPs, EDC4 could have a role in basal p62 droplets. Immunogold electron microscopy (EM) further indicated that DDX6 was localized at puromycin-enlarged p62 droplets (Figure 2D). p62 droplets with the PBy marker EDC4 contained mRNAs, as probed by oligo(dT)30 (Figure 2E). CHX, which blocks cytoplasmic RNP granule formation,[41,42] consistently abolished puromycin-enlarged p62 droplets containing DDX6 (Figure S2C).

We further ruled out the possibility that the full recruitment of PB-specific markers by p62 droplets was due to p62 promiscuously binding to globally polyubiquitinated proteins under puromycin treatment, which may enhance protein polyubiquitination. First, puromycin-enlarged p62 droplets did not colocalize with SGs marked with G3BP1, Caprin-1, or G3BP2 (Figure 1E). Second, under puromycin treatment, the colocalization of several other non-RBPs and YTHDF3 with p62 droplets was negligible (Figure S1F). Third, mutant huntingtin (mHTT) with a polyglutamine (polyQ) expansion induces proteotoxicity, causing Huntington's disease (HD).[43] mHTT with 103Q also promoted the colocalization of p62 droplets and EDC4, inducing the formation of enlarged p62/EDC4 droplets that mark enlarged PBs, in inducible mHTT-stably expressing cells (Figure 2F). Finally, in self-renewing tissue-resident macrophages (Max Planck Institute [MPI] cells),[44] LPS, an endotoxin, induced the formation of p62-associated enlarged PBs, while oxidation with H_2O_2 maximized the effect of LPS. The levels of p62-associated PBs appeared to correlate with the levels of p62 (Figure 2G). LPS stimulates the expression of inflammatory proteins, including nuclear factor κB (NF-κB) and IRF-3, inducing proinflammatory responses in macrophages, monocytes, and endothelial cells,[45] and NF-κB activation induces p62 expression.[46] These data indicate that, under proteotoxicity, endotoxicity, or oxidation, autophagic p62 droplets are converted to PBs.

It is tempting to address the fate of normal PBs and how normal PBs and p62 droplets are incorporated under stress conditions. Normal-sized PBs that exist under basal conditions did not disappear under stress conditions (Figure S2D). This suggests that, under stress conditions, normal PBs are not dissolved but incorporated into p62 droplets. Furthermore, GFP-DDX6 puncta appeared to fuse with p62 droplets under puromycin treatment (Figure S2E), suggesting that normal PBs fuse with p62 droplets to become enlarged RNP granules.

p62 and critical RBPs are essential for the nucleation of proteotoxic stress-enlarged PBs

To address whether p62 and critical RBPs are necessary for the nucleation of stress-induced enlarged PBs, we employed proteotoxicity as a model of stress. p62 knockdown largely reduced the levels of PBs, marked with EDC4, under proteotoxic stress as well as basal conditions (Figure 3A). Consistently, p62 knockout (KO) almost entirely abolished enlarged PBs (Figure 3B). Likewise, EDC4-marked PBs were largely lost in p62 KO HAP1 cells (Figure S3A). p62 depletion did not significantly impact EDC4 protein levels, while EDC4 knockdown appeared to mildly reduce p62 protein levels (Figure S3B). These data suggest that p62 is required for the formation of the proteotoxicity-enlarged PBs, termed pd-PBs, as opposed to constitutive PBs.

De novo formation and maintenance of PBs depend on the concentrations of mRNAs and many RBPs of PBs. EDC4,[47] LSM14A,[48] and DDX6[49,50] are among these critical RBPs, given that their low-complexity domains are needed for LLPS. We questioned whether the essential mRNA-binding components of PBs play crucial roles in proteotoxic stress-induced p62 droplet formation. Ablation of EDC4 effectively blocked p62 droplet formation (Figure 3C). EDC4 had two pools in cells under basal conditions: a pool of EDC4 in basal PBs and another in basal p62 droplets (Figure S3C; see also Figure 2C). This suggests that EDC4 could be involved in basal p62 droplet formation. Indeed, while EDC4 knockdown abolished pd-PB formation (Figure 3C), EDC4 in basal p62 droplets appeared to be critical for p62 droplet formation, as knockdown of EDC4 also reduced basal p62 droplet formation (Figure 3C). Presumably, EDC4 would help nucleate basal p62 droplets that function as the pre-structures of pd-PBs. Notably, although ablation of p62 reduced the overall size of p62/EDC4-positive droplets (Figures 3A and 3B), it did not appear to influence EDC4-only-decorated PBs that are independent of p62 (Figures S3D and S3E).

By contrast, under basal conditions, LSM14A had only one pool in basal PBs, and it did not colocalize with basal p62 bodies (Figure S3C; see also Figure 2B) but entirely colocalized with p62 in pd-PBs under proteotoxicity (Figures 2B and S4A). Knockdown of LSM14A entirely abolished proteotoxic stress-induced p62 droplet formation, although it did not affect basal p62 droplet formation (Figure S4A). Reciprocally, p62 depletion did not significantly reduce basal DDX6 or LSM14A droplets (Figure S4B), which do not effectively colocalize with p62 droplets under basal conditions. The fact that p62 ablation did not affect basal PBs (Figures S3D, S3E, and S4B) suggests that p62 is dispensable for basal PBs, while it is essential for the formation of stress-induced pd-PBs. The reciprocal roles of p62 and PBs' crucial components in proteotoxic stress-induced PBy nucleation/p62 droplet formation indicate that p62 and critical RBPs cooperatively determine the nucleation of pd-PBs, strengthening the conclusion that stress-enlarged p62 droplets represent a type of PBs: pd-PBs.

p62 droplet seeding drives the nucleation of pd-PBs

We aimed to understand why p62 was required for the formation of pd-PBs. LPS induced p62 expression, p62 droplet

with EDC4 droplets greater than 1 μm was quantified. n = 50 cells. 100% of cells with CFP-103Q aggregates, but none of the cells without CFP-103Q aggregates, have EDC4 droplets with diameters greater than 1 μm.

(G) MPI cells were treated as indicated. The cells were stained with anti-p62 and anti-EDC4. Confocal images were acquired. Immunoblotting indicates p62 levels. The percentage of cells with p62-associated enlarged PBs was quantified. n = 3 independently plated wells.

Statistical analysis was performed by one-way ANOVA with Bonferroni multiple-comparisons test. The F/degree of freedom/post hoc p values are indicated. ***$p < 0.0001$. The areas boxed in yellow are magnified. Scale bars, 10 μm and 2 μm (magnification) (A–C and E–G).

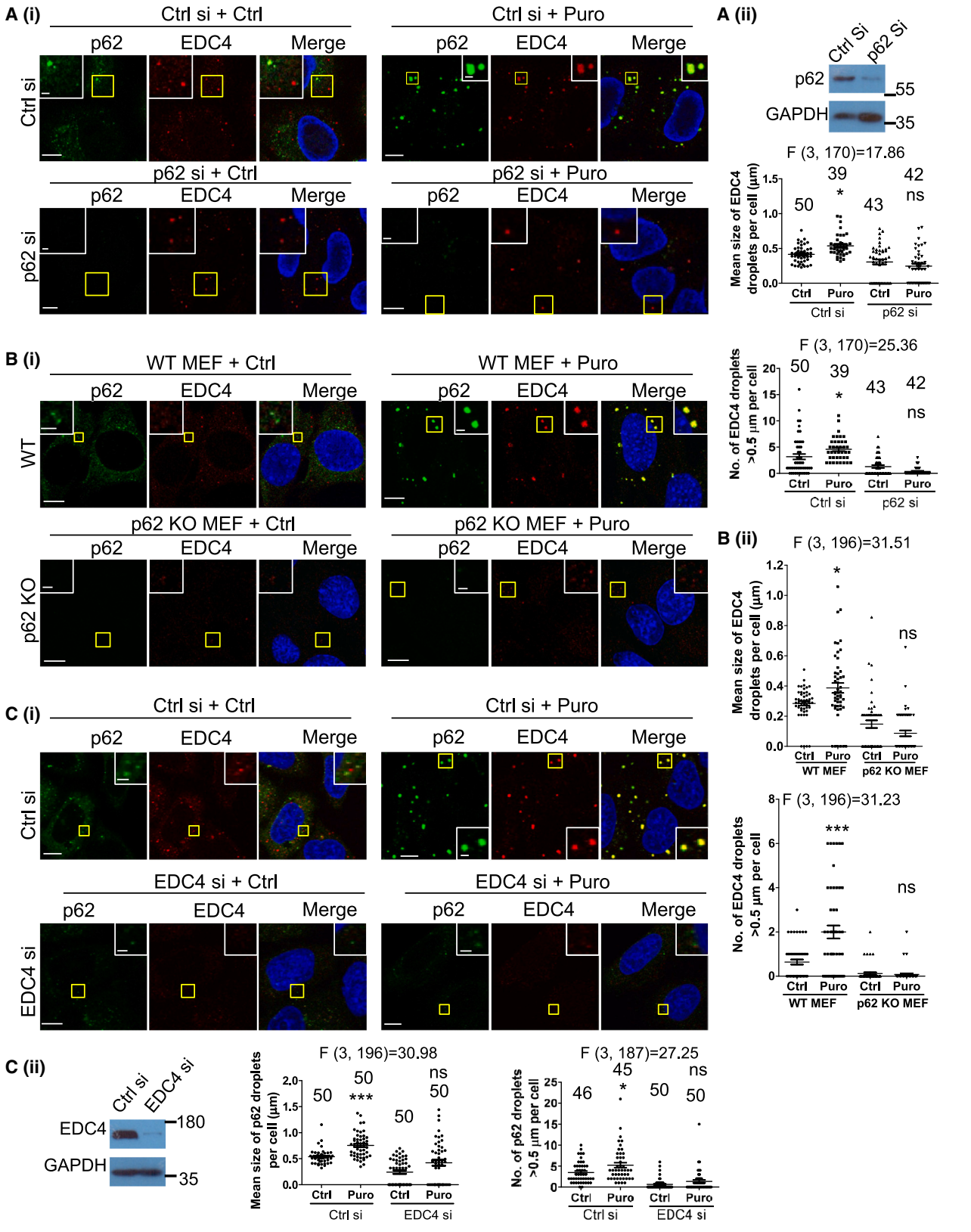

(legend on next page)

formation, and pd-PB formation in MPI cells (Figure 2G), suggesting that p62 droplet formation may drive pd-PB formation. Polyubiquitin binding to p62 is critical for p62 to cluster into droplets.[2,3] The PB1 domain localized at the p62 N terminus is required for p62 oligomerization,[51,52] and the ubiquitin-associated (UBA) domain at the p62 C terminus interacts with polyubiquitin chains on polyubiquitinated proteins.[40] This allows us to test the establishment of pd-PBs by modulating p62 droplet formation. In p62 KO cells, GFP-p62ΔPB1 and the GFP-p62 N terminus (p62-1–256 amino acids [aas]) were unable to colocalize with pd-PBs marked with GW182 (Figures 4A and 4B) or EDC4 (Figure S5A), but GFP-full-length p62 was able to colocalize (Figures 4A and S5A). This implies that the p62 C terminus (p62-C) would be necessary for the formation of pd-PBs. We have shown that p62-N (1–256aa) alone does not tend to form droplets under basal conditions but colocalizes with full-length p62 and reduces the size of full-length p62 droplets.[53] Indeed, in p62 knockdown cells, puromycin-induced p62-N puncta were unable to colocalize with EDC4 and nucleate EDC4-marked PBs (Figure S5B, right), whereas p62-N in control knockdown cells was able to do so under proteotoxic stress conditions because p62-N colocalized with endogenous full-length p62 that was capable of nucleating EDC4 (Figure S5B, left). These data confirmed that p62-C with the UBA domain was required for *de novo* formation of pd-PBs. We hypothesized that p62 droplet formation elicited by polyubiquitin binding is a driving force for the formation of pd-PBs. Consistent with the hypothesis, the chemical inhibitor TAK-243, which blocks protein ubiquitination by selectively inhibiting the ubiquitin-activating enzyme(UAE/E1) activity,[54,55] halted the formation of puromycin-induced pd-PBs (Figure 4C). p62 mutation M404V is known to be associated with Paget's disease of bone (PDB),[56] and p62 P392L is associated with both ALS-FTLD[34] and PDB.[56] M404 locates at the UBA-polyubiquitin interaction interface, whereas P392 is at a more distant position. The M404V mutation modifies the putative polyubiquitin-binding van der Waals surface, abolishing the ability to bind polyubiquitin chains, while the P392L mutant binds polyubiquitin chains normally, although it appears to affect monoubiquitin chain binding.[56] Therefore, p62 M404V, defective in binding to polyubiquitin chains, is unable to form p62 droplets.[2] Indeed, p62 M404V was unable to nucleate EDC4 in p62 knockdown cells treated with puromycin (Figure 4D). The p62 P392L mutation, which does not alter p62's polyubiquitin chain binding, did not affect the formation of pd-PBs under puromycin treatment (Figure 4D). Our data show that proteotoxic stress accumulates polyubiquitinated proteins, which lead to enhanced p62 droplet formation, thus facilitating nucleation of pd-PBs. This supports the concept that p62 droplet formation drives the formation of pd-PBs in stressed cells.

p62 phase separation driven by polyubiquitin chains promotes DDX6 clustering *in vitro*

In our BioID2 screening, the PB component DDX6 (a DEAD-box ATPase) was identified as a p62 proximity protein (Figures 1A and 1F). DEAD-box ATPases have been reported to be global regulators of phase-separated organelles.[57] We observed that p62 physically interacted with DDX6 (Figures 5A and 5B). The fact that the migration rate of DDX6 with 54 kD is close to that of the antibody heavy chain, which usually bears 55 kD, precludes an immunoprecipitation assay of the endogenous p62-DDX6 interaction. To test whether p62 modulates DDX6 clustering *in vitro*, we initially characterized the conditions for DDX6 droplet formation and found that polyU, ATP, and salt concentration were critical for DDX6 clustering (Figure S6A). polyU appeared to be important to maintain the droplet state of DDX6, while ATP promoted DDX6 phase transition (Figures S6B and S6C). We thus established a condition (0.5× basal phase separation buffer [BPSB]), under which GFP-DDX6 alone formed a minimum of droplets. p62 modestly promoted DDX6 droplet formation under the condition (Figures 5C and 5D). Polyubiquitinated proteins are known to drive p62 droplet formation.[2,3] In the presence of both polyubiquitin chains and p62, DDX6 underwent rapid condensation and gelation (Figure 5D, bottom right), as shown previously.[57] We separated droplets from the phase separation solution by sedimentation and determined the levels of GFP-DDX6 and p62 in each fraction by immunoblotting. Figure 5E confirms that the mixture with p62 and polyubiquitinated proteins yielded more GFP-DDX6 protein in the pellets than the mixture containing no p62 or polyubiquitinated proteins. The *in-vitro*-reconstituted system suggests that polyubiquitin chain-driven p62 droplets condense DDX6 inside them. Subsequently, we confirmed these data in cells. While puromycin, which increases cellular polyubiquitination, caused increased DDX6 condensation in cells with control small interfering RNA, it failed to enhance DDX6 condensation in p62 knockdown cells (Figure S6D). This supports the theory that protein polyubiquitination, which drives p62 phase separation, is critical for pd-PB formation. These assays indicate that polyubiquitin chain-driven p62 droplet formation promotes DDX6 clustering, supporting our conclusion that enlarged pd-PB formation is driven by enhanced p62 droplet formation, which occurs under proteotoxic and other stress conditions (Figure 5F).

Figure 3. p62 or PBy components are essential for the formation of pd-PBs

(A) HeLa cells were knocked down with Ctrl or p62 siRNA. After 24 h, the cells were split, and after another 24 h, the cells were treated with Ctrl or Puro for 3.5 h. The cells were stained for p62 and EDC4. The immunoblot shows the p62 siRNA knockdown efficiency. EDC4 droplet sizes per cell were quantified with ImageJ. The mean sizes and the number of EDC4 droplets with diameters greater than 0.5 μm per cell are shown. n = 39–50 cells, as indicated.

(B) Wild-type (WT) or p62 KO mouse embryonic fibroblasts (MEFs) treated with Ctrl or Puro were co-stained with the antibodies for p62 and the PBy marker EDC4. The mean sizes and the number of EDC4 droplets with diameters greater than 0.5 μm per cell are shown. n = 50 cells.

(C) HeLa cells were knocked down with Ctrl or EDC4 siRNA. The cells were stained for p62/EDC4. The immunoblot shows the EDC4 siRNA knockdown efficiency. The mean sizes and the number of p62 droplets with diameters greater than 0.5 μm per cell are shown. n = 45–50 cells as indicated. Confocal images were acquired. The area boxed in yellow is magnified.

Scale bars, 10 μm and 2 μm (magnification). Data are shown as mean ± SEM. Statistical analysis was performed by one-way ANOVA with Bonferroni multiple-comparisons test. The F/degree of freedom/post hoc p values are indicated. *p < 0.05, ***p < 0.0001.

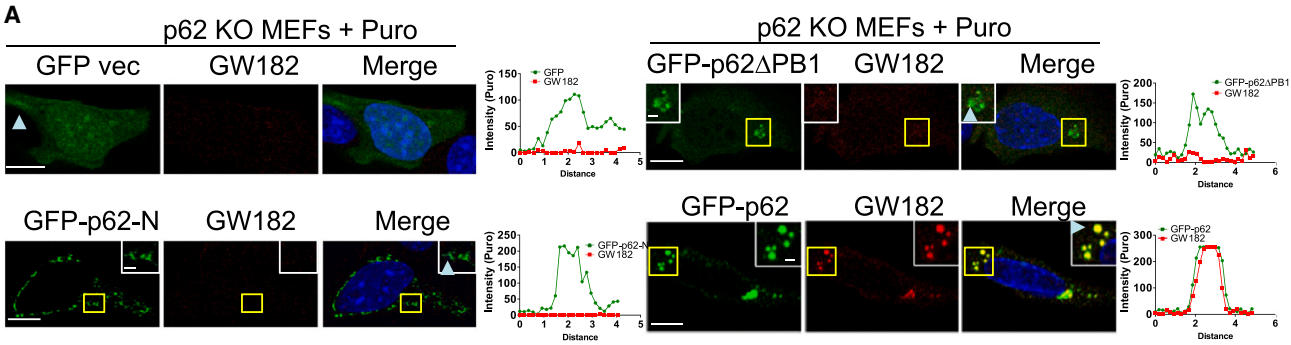

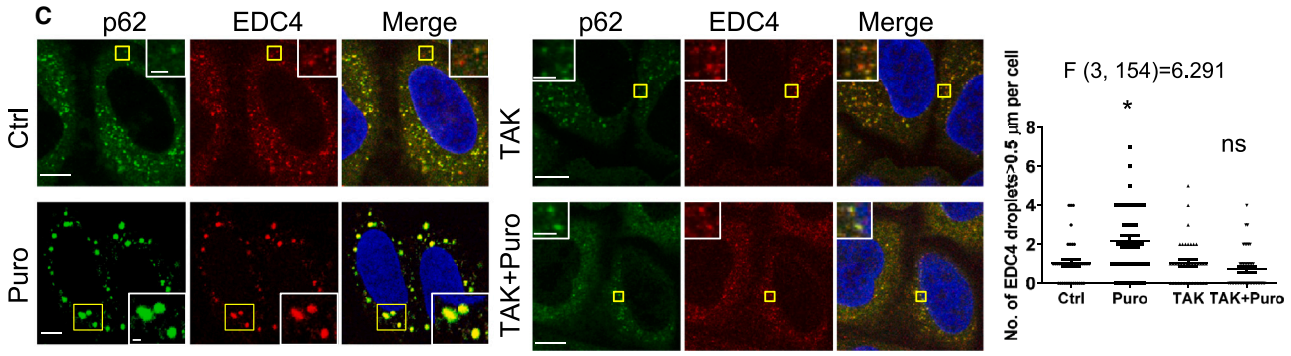

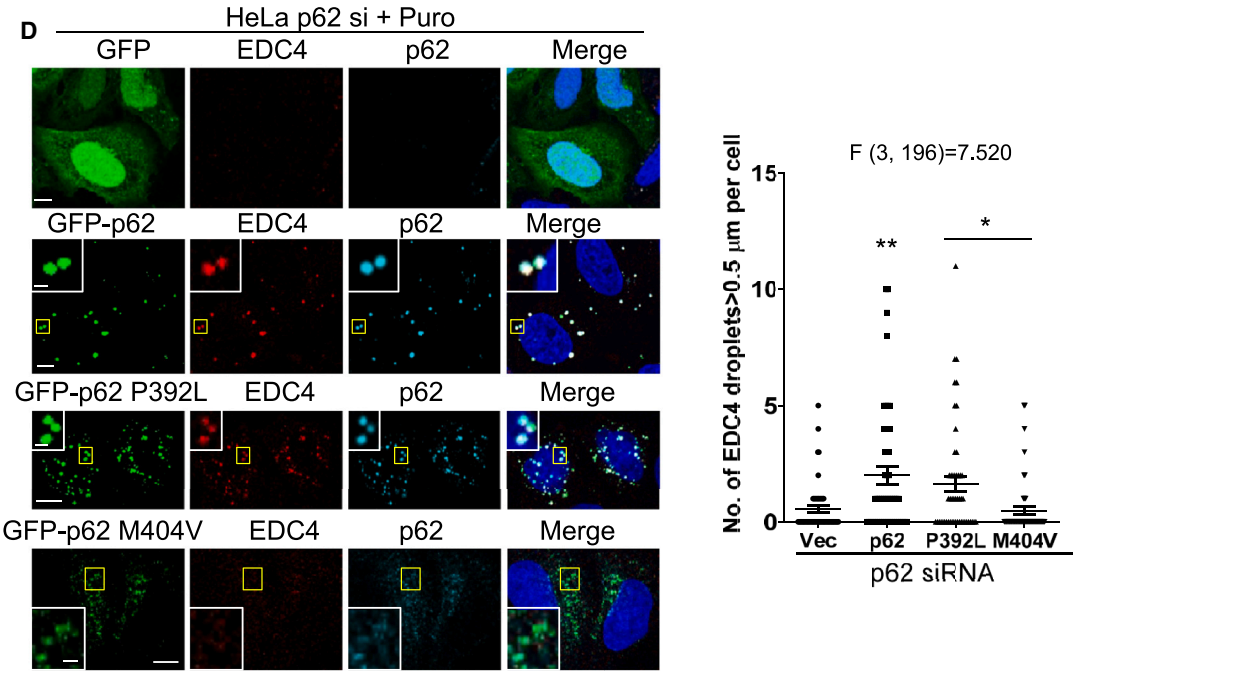

(legend on next page)

pd-PBs serve as platforms to regulate the formation of NLRP3 inflammasomes

LPS endotoxicity induces the formation of pd-PBs (Figure 2G). Stimulation by LPS and oxidation caused a strong induction of pd-PBs in primary bone marrow-derived macrophages (BMDMs) (Figure 6A). We determined the role of H_2O_2 oxidation in promoting pd-PBs in MPI cells, primary tissue-resident macrophages that do not undergo oncogenic transformation, exhibiting properties of alveolar macrophages.[44] H_2O_2 oxidation markedly enhanced the effect of LPS on the formation of pd-PBs, promoting the size of pd-PBs (Figure 6B). We thus aimed to investigate p62-binding proteins by p62 immunoprecipitation in LPS-primed MPI cells using liquid chromatography-tandem mass spectrometry (LC-MS/MS). Among the identified p62-binding candidates (Table S2), ASC/PYCARD, a pyrin- and CARD-domain containing protein (Figure S7A), came to our attention due to its critical role in inflammasome formation.[36] We validated the endogenous ASC-p62 interaction (Figure 6C). LPS and nigericin, which initiate the priming signal (signal 1) and activation signal (signal 2), respectively, induce ASC/NLPR3 inflammasome formation.[58] p62 droplets did not colocalize with ASC under basal conditions (Figures S7B and 6D), but LPS+nigericin treatment caused the recruitment of ASC by induced pd-PBs in BMDMs (Figure 6D). We employed MPI cells to further define the role of nigericin in ASC recruitment by pd-PBs. LPS-induced pd-PBs modestly colocalized with ASC; however, nigericin led to the profound colocalization of ASC with pd-PBs. In the presence of nigericin, LPS+H_2O_2 treatment-induced pd-PBs virtually nucleated all cellular ASC (Figures 6E and S7B). However, basal PBs marked by DDX6 or EDC4 did not colocalize with ASC (Figure S7C). On the other hand, basal p62 droplets did not colocalize with ASC (Figure S7B). These data suggest that pd-PBs specifically recruit ASC and activate its downstream signaling. Of note, LPS+H_2O_2 markedly increased p62 protein levels (Figure S7D). The increased p62 levels in stress settings would contribute to pd-PB recruitment of ASC, although we do not exclude the possibility that p62 or ASC protein modifications could be involved in the recruitment of ASC by pd-PBs.

pd-PBs promote NLRP3 inflammasome activation

We observed that NLPR3 and caspase-1 were assembled into pd-PBs in MPI cells under LPS+nigericin treatment (Figures 7A and 7B). This suggests that pd-PBs could serve as platforms for the formation of inflammasomes. Of note, p62 has been reported to ameliorate NLRP3 inflammasome activation via mitophagy[46] and attenuation of ROS production,[59] while we predict that the pd-PB role of p62 should promote NLRP3 inflammasome activation. The multiple roles of p62 may simultaneously regulate NLRP3-dependent inflammation. Indeed, p62 knockdown enhanced LPS+nigericin-induced cytotoxicity and promoted interleukin-1β (IL-1β) production (Figures S8A and S8C) rather than reducing NLPR3 inflammasome activation. The data obtained from p62 knockdown presumably indicate the overall effect of p62 on alleviation of IL-1β production, given the diverse roles of p62 in NLRP3 inflammasome activation.

We hoped to examine the specific role of pd-PBs in NLRP3 inflammasome activation by eliminating the confounding effect from the anti-oxidation role of p62 with blockade of ROS production. However, addition of N-acetyl-L-cysteine (NAC), a ROS scavenger, rescued LPS and nigericin-induced toxicity in cells with either control or p62 knockdown, and NAC treatment abrogated the increase in LPS/nigericin cytotoxicity by p62 knockdown (Figure S8D). NAC appeared to mask all effects of p62 on NLRP3 inflammation toxicity, likely because NAC blocks the proinflammatory response in LPS-stimulated macrophages.[60] Thus, technically, it is unfeasible to separate the putative role of pd-PBs in NLRP3 inflammasome activation from other roles of p62 in inhibiting NLRP3-dependent inflammation, including those of pro-mitophagy and anti-oxidation of p62.

Although it is not practical to test the specific role of pd-PBs in NLRP3 inflammasome activation by p62 knockdown, due to the complex role of p62 in inflammation, we validated the role of pd-PBs in NLRP3 inflammasome activation by ablation of PB formation. We thus knocked down EDC4, DDX6, or LSM14A to eliminate pd-PBs, given that these RBPs are critical for the formation of PBs.[47,48,50] Knockdown of EDC4, LSM14A, or DDX6 (Figure S8E) ameliorated caspase-1 activation and GSDMD cleavage in MPI cells (Figure 7C). ASC recruitment into pd-PBs was critical for caspase-1 localization to pd-PBs, as knockdown of ASC abolished the recruitment of caspase-1 by pd-PBs as the NLRP3 downstream signaling (Figure S9A). Consistently, knockdown of EDC4, DDX6, or LSM14A reduced LPS+nigericin-induced NLRP3 inflammasome cytotoxicity (Figure 7D). We confirmed that DDX6 or EDC4 knockdown did not significantly influence the protein levels of NLRP3 and ASC (Figures S9B and S9C). Furthermore, knockdown of these PB components significantly reduced the production of IL-1β (Figure 7E). Our data show that pd-PBs sequester ASC, thereby facilitating the assembly of NLRP3 inflammasomes (Figure 7F). Transformation of p62 bodies to pd-PBs upon endotoxin stress acts as a stress response to induce inflammasome activation. Interestingly, in addition to the pro-inflammation of pd-PBs, p62 also exerts

Figure 4. p62 droplet formation drives PB nucleation

(A) WT or p62 KO MEFs were transfected with GFP vector Ctrl, GFP-p62 with PB1 deletion (GFP-p62-ΔPB1), GFP-p62-N-1–256 (GFP-p62-N), or GFP-p62. After 20 h, the cells were treated with Puro for 3.5 h. The cells were stained with p62 and GW182 antibodies. Confocal images were acquired. p62/GW182 colocalization in the droplet (indicated by the arrowhead) was quantified by line profiling.

(B) Schematic domain architecture of p62, p62ΔPB1, and p62-N. Note that the C-terminal UBA domain of p62 is located at residues 387–436.

(C) HeLa cells were pre-treated with Ctrl or TAK-243 (1 μM) overnight, and the pre-treated cells were subjected to Ctrl or Puro treatment for 3.5 h. The cells were stained for p62 and EDC4. The number of EDC4 droplets with diameters greater than 0.5 μm per cell are shown. n = 40 cells.

(D) HeLa cells were knocked down with p62 siRNA. After 24 h, the cells were split, and after another 24 h, the cells were transfected with GFP vector Ctrl, GFP-p62, GFP-p62 P392L, or GFP-p62 M404V. After 20 h, the transfected cells were treated with Puro for 3.5 h. The cells were then fixed and stained with p62 and EDC4 antibodies. Confocal images were acquired. The number of EDC4 droplets with diameters greater than 0.5 μm per cell is shown. n = 50.

Scale bars, 10 μm and 2 μm (magnification) (A, C, and D). Statistical analysis was performed by one-way ANOVA with Bonferroni multiple-comparisons test. Data are shown as mean ± SEM. The F/degree of freedom/post hoc p values are indicated. *$p < 0.05$, **$p < 0.01$, ***$p < 0.0001$ (C and D).

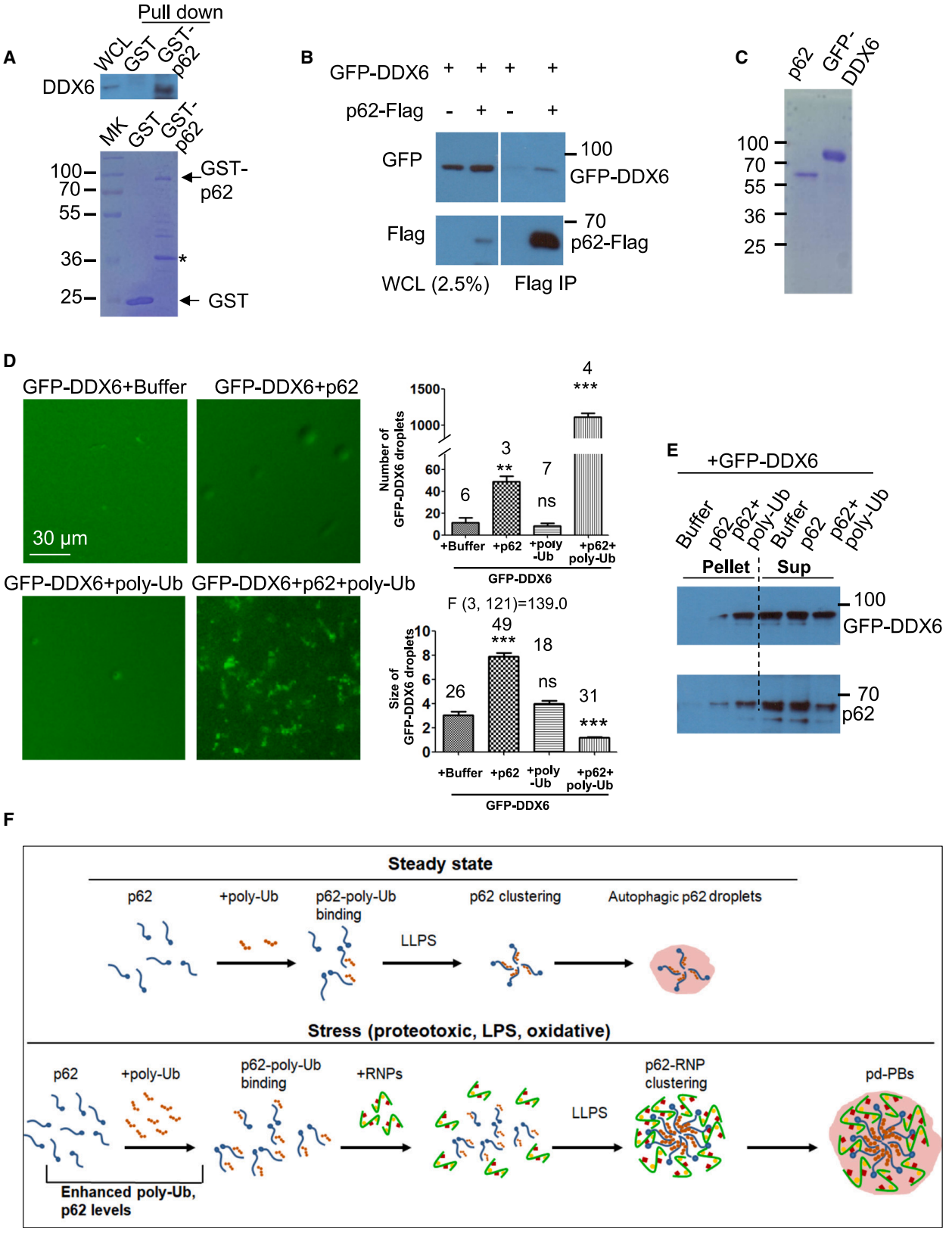

(legend on next page)

anti-inflammation through pro-mitophagy and anti-oxidation, as aforementioned. The dual role of p62 for positive and negative regulation of NLRP3-dependent inflammation may be important to maintain the homeostasis of NLRP3 inflammasome activation.

DISCUSSION

Our study unveils that, under a variety of stresses, autophagic p62 droplets are selectively converted to pd-PBs, suggesting a previously unexplored role of p62 in PB condensation. The transformation of p62 droplets to pd-PBs positively regulates NLRP3-dependent inflammation, with pd-PBs assembling NLRP3 inflammasomes. Notably, even under basal conditions, autophagic p62 droplets can partially overlap with EDC4, while all tested PB markers, including Dcp1a, LSM14A, and DDX6 as well as EDC4, almost wholly enter proteotoxic stress-enlarged p62 bodies. This suggests that EDC4 may nucleate at the pre-structures of pd-PBs, while Dcp1a, LSM14A, and DDX6 localize at mature pd-PBs. Autophagic p62 droplets along with EDC4, in addition to their role in selective autophagy, may function as pre-structures poised for proteotoxic stress-induced pd-PB formation (Figure S9D). At present, it is unclear whether pd-PBs can be cleared by autophagy. Intriguingly, it has been reported that p62 condensates sequester translation initiation factors and mediate autophagy of eIF2a and eIF4E.[61] It would be interesting to investigate whether pd-PBs are preferred substrates of autophagy.

Selective role of p62 for *de novo* formation of pd-PBs

RNP granule formation depends on weak interactions between untranslated RNAs and RNAs, proteins and proteins, or proteins and RNAs through their IDRs or well-folded domains.[11] Although hundreds of proteins and thousands of RNAs have been revealed as constituents of RNP granules, including PBs and SGs, the basis for the assembly and maintenance of RNP granules has not been well understood. Depletion of many RBPs that are capable of LLPS *in vitro* did not show a significant impact on the assembly of RNP granules, of which the RBPs consist.[9] Among hundreds of component proteins of SGs, only untranslated preinitiation complexes and limited RBPs are required for the establishment of the stable core of the granules. Under stress, p62 droplet seeding selectively drives the nucleation of PBs rather than SGs. Multivalency is a key determinant to regulate biomolecular condensate formation. IDRs are critical for the availability of valency. According to IPUred3 analysis, there are two potential IDRs in p62, which potentially serve as a source of multivalent interactions for the assembly of PBs. Our data show that binding of its UBA domain to polyubiquitin chains is important to nucleate pd-PBs.

Transformation of autophagic p62 droplets to pd-PBs upon stress regulates the NLRP3 inflammasome

Proteotoxicity, which enhances the levels of polyubiquitinated proteins, transforms p62 droplets into pd-PBs. We conclude that the increase in the levels of polyubiquitinated proteins promotes p62 droplet formation, which subsequently drives LLPS of pd-PBs. The mechanism could facilitate the disassembly of stress-induced PBs upon withdrawal of stress, conferring the dynamics of pd-PBs. By contrast, ubiquitination has been shown recently to be required for the disassembly of SGs.[24]

In macrophages, endotoxin stress induces the formation of pd-PBs, as it induces NF-κB activation[45] and p62 expression,[46] leading to enhanced p62 droplet formation. H_2O_2 oxidation potentiates the effect of LPS on p62 expression and pd-PB formation (Figure 6B), and nigericin promotes ASC recruitment by pd-PBs (Figure 6F). Our data indicate that pd-PBs serve as platforms to positively regulate the formation of NLRP3 inflammasomes. On the other hand, p62 may ameliorate NLRP3 inflammasome activation via pro-mitophagy[46] and attenuation of ROS production.[59] The anti-inflammation role of p62 could halt NLRP3 inflammasome hyperactivation of pd-PBs to prevent cellular overinflammation under persistent stress. Yin and yang of p62 in NLRP3-dependent inflammation may be necessary to maintain the homeostasis of NLRP3-dependent inflammation.

Persistent pd-PBs in neuroinflammation toxicity

Protein misfolding is a hallmark of neurodegenerative diseases. Neuronal protein aggregation enhances neuroinflammation, resulting in inflammation-associated neurotoxicity.[62] It is not well characterized how protein misfolding causes neuroinflammation. Our study suggests that the formation of pd-PBs fueled by misfolding proteotoxicity may contribute to

Figure 5. p62 promotes DDX6 clustering *in vitro* in a polyubiquitin chain-dependent manner

(A) HeLa cell lysates were subjected to pull-down by recombinant glutathione S-transferase (GST) or GST-p62. Bacterially expressed GST or GST-p62 was pulled down with glutathione beads. GST- or GST-p62-bound beads were incubated with HeLa cell lysates. The pull-down products and the whole-cell lysates (WCLs) were probed with anti-DDX6. An aliquot of GST or GST-p62 bound beads was subjected to SDS-PAGE. An asterisk denotes a breakdown product of GST-p62. MK, protein marker.

(B) GFP-DDX6/vector or GFP-DDX6/p62-FLAG was transfected into HeLa cells. The cell lysates were immunoprecipitated with anti-FLAG agarose beads. The WCLs and immunoprecipitates were used for immunoblotting with anti-GFP and anti-FLAG antibodies successively.

(C) The purified recombinant p62 and GFP-DDX6.

(D) GFP-DDX6, GFP-DDX6+p62, GFP-DDX6+polyubiquitinated proteins (poly-Ub), or GFP-DDX6+p62+poly-Ub was subjected to *in vitro* phase separation in a microcentrifuge tube. A 4 μM final concentration of GFP-DDX6 was maintained in 0.5× BPSB. Where appropriate, a 1 μM final concentration of p62 and/or a 0.75 μM final concentration of poly-Ub was added. The phase-contrast images were acquired with a Leica DMi8 microscope. Scale bar, 30 μm. The number of GFP-DDX6 droplets in each image (460 × 620 μm) was scored (LAS-X). n = 3–7 images for each group, as indicated. The size of GFP-DDX6 droplets was assessed (LAS-X). n = 18–49 droplets, as indicated. Data are shown as mean ± SEM. Statistical analysis was performed by two-tailed unpaired t test (**p = 0.0013, *** p < 0.0001; not significant (ns), p = 0.5643; top) or by one-way ANOVA with Dunnett's multiple-comparisons test. The F/degree of freedom/post hoc p values are indicated. ***p < 0.0001 (bottom).

(E) A mixture (30 μL) of GFP-DDX6 protein (with Ctrl buffer), p62+GFP-DDX6, or p62+GFP-DDX6+poly-Ub was subjected to *in vitro* phase separation. The pellet and supernatant (Sup) were probed by immunoblotting with the indicated antibodies.

(F) The proposed model for p62 driving the assembly of PB condensates under stress conditions: p62 and RNPs co-operatively form pd-PBs.

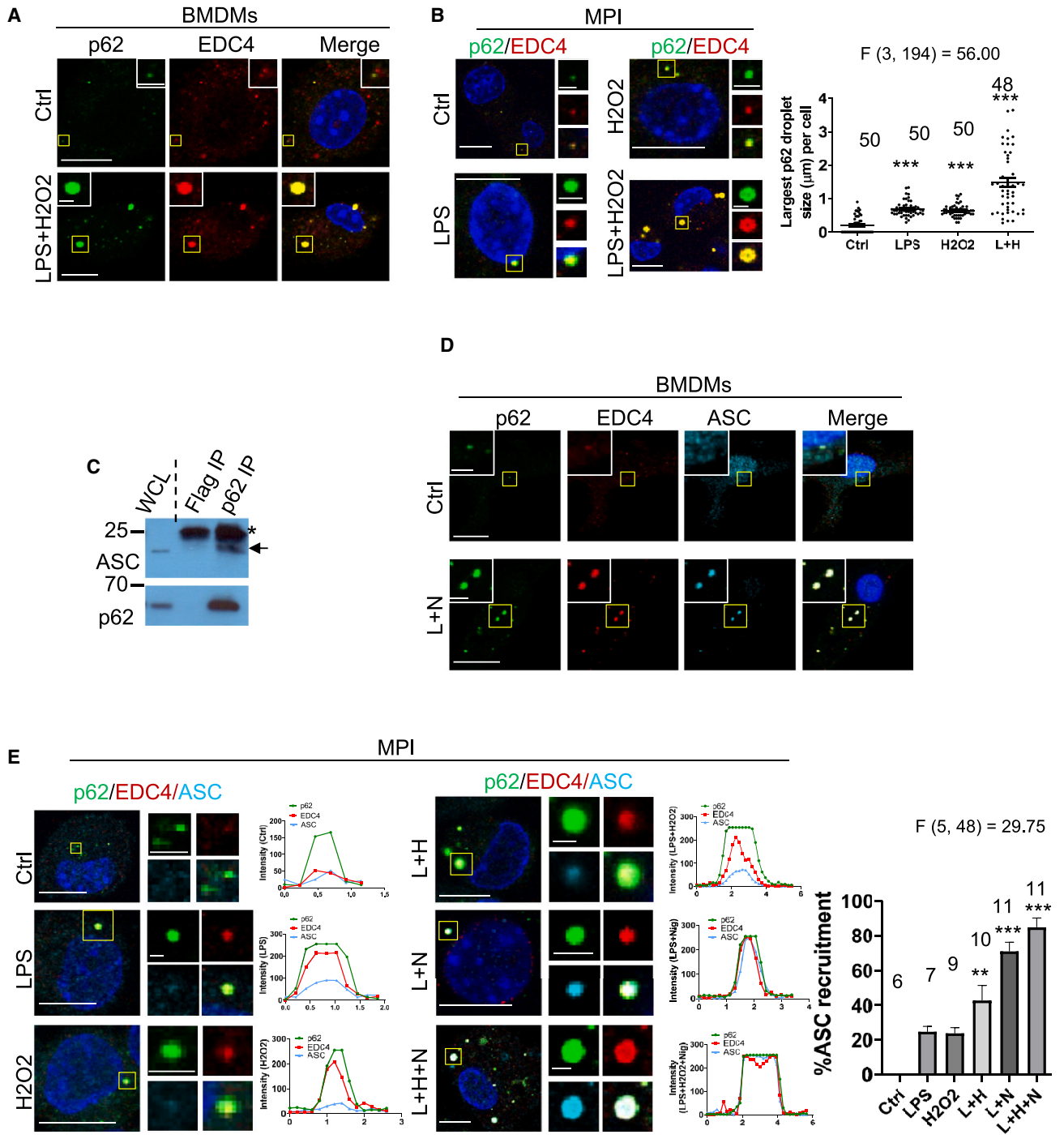

Figure 6. pd-PBs recruit ASC, the adaptor of NLRP3 inflammasomes

(A and B) H_2O_2 promotes LPS-induced pd-PB formation. BMDMs (A) or MPI macrophages (B) were treated as indicated. Cells were stained with anti-p62 and anti-EDC4. The sizes of p62 droplets were quantified. n = 50 or 48 cells as indicated (B).

(C) Identifying ASC as a binding partner in macrophages. MPI cells were treated with LPS, and cell lysates were immunoprecipitated with anti-p62. Immunoprecipitates were probed by anti-ASC and anti-p62 successively in western blots. The arrow indicates the signals of ASC, and an asterisk marks antibody light chains (~25 kD).

(legend continued on next page)

neuroinflammation in neurodegenerative diseases. RNP granules such as PBs and SGs are involved in regulating RNA storage, metabolism, and translational repression.[5,6] The dynamics of RNP granules are critical for cellular homeostasis. Upon the withdrawal of stress stimuli, RNP granules disassemble in a rapid manner to maximally avoid protein aggregation and RNA toxicity.[32,63] Mutations in IDRs of RBPs stabilizing RNP granules can cause RNA toxicity and correlate with the ALS-FTLD spectrum.[26–32] Persistent pd-PBs may result in enhanced NLRP3-dependent inflammation and toxicity. Interestingly, numerous p62 mutations are found in the patients with ALS and FTLD.[34] Mutations in p62 could remodel the nucleation of pd-PBs, promoting the assembly of NLRP3 inflammasomes by recruitment of ASC. Future studies will characterize whether ALS/FTLD-associated p62 mutations alter the dynamics of pd-PBs and, in turn, contribute to the mutation-associated neuroinflammation toxicity.

In this study, we revealed that autophagic p62 bodies are transformed into pd-PBs upon certain stresses. In macrophages, pd-PBs activate inflammation by sequestering ASC. pd-PBs may act as a signaling hub of the stress response to maintain cellular homeostasis. It is warranted to unravel additional functions of pd-PBs under various cellular and environmental settings.

Limitations of the study

Previously, valosin-containing protein (VCP) has been shown to mediate the clearance of SGs by autophagy.[9] The selective clearance of PBs by autophagy has not been elucidated. Here we did not demonstrate whether p62 also mediates the autophagic clearance of pd-PBs. Further investigation will clarify the possible role of p62 in autophagic clearance of pd-PBs.

STAR★METHODS

Detailed methods are provided in the online version of this paper and include the following:

- KEY RESOURCES TABLE
- RESOURCE AVAILABILITY
  - Lead contact
  - Materials availability
  - Data and code availability
- EXPERIMENTAL MODEL AND SUBJECT PARTICIPANT DETAILS
  - Culture of cell lines
  - Culture of primary BMDMs
- METHOD DETAILS
  - Drug treatment
  - DNA cloning and mutagenesis
  - siRNAs
  - DNA and siRNA transfection
  - BioID2
  - Liquid chromatography and tandem mass spectrometry
  - Global protein translation assay
  - Fluorescence recovery after photo bleaching (FRAP)
  - Immunocytochemistry
  - Immunogold labeling
  - RNA Fluorescent *in situ* hybridization (FISH)
  - Hybridization mixture for a sample (80 μL per coverslip)
  - Generating lentivirus and transduction
  - Western blot analysis
  - 6 × his-tagged protein expression and purification
  - Immunoprecipitation
  - Polyubiquitinated protein purification
  - *In vitro* DDX6 phase-separation
  - *In vitro* sedimentation assays
  - LDH cytotoxicity
  - ELISA
  - Gene Ontology (GO) analysis
- QUANTIFICATION AND STATISTICAL ANALYSIS
  - Particle analysis for cellular protein droplets
  - Statistical analysis

SUPPLEMENTAL INFORMATION

Supplemental information can be found online at https://doi.org/10.1016/j.celrep.2024.113935.

ACKNOWLEDGMENTS

We thank Dr. M. Komatsu for p62 KO and control MEFs and Dr. A. Yamamoto for CFP-HTT (exon 1)-103Q HeLa Tet-off cells. We are grateful to Dr. D. Rubinsztein for critical advice. This work was supported by Medical Research Council UK MR/M023605/1 (to S.L.), Rosetrees Trust PGL21/10002 (to S.L.), BRACE Charity BR17/4 (to S.L.), UK Academy of Medical Sciences and Newton Fund for Newton Advanced Fellowship NAF\R1\191045 (to B.L. and S.L.), Royal Society IEC\NSFC\191180 (to S.L.), National Natural Science Foundation of China 91649105 (to B.L.), and National Key Research and Development Program of China 2016YFC0905100 (to B.L.).

AUTHOR CONTRIBUTIONS

S.L. conceived the project, analyzed the data, and wrote the manuscript. E.R.B. and E.V. performed the majority of the experiments. C.R.B. performed immunocytochemistry and data quantification. Y.Y., S.H., and W.A.O. conducted immunoblotting and cell culture experiments. A.S. performed immunogold experiments and electron microscopy imaging. J.L. contributed to the culture of MPI cells and BMDMs and ELISA experiments. W.W. contributed to isolation of BMDMs. H.N.S. helped with experiments and participated in discussions. G.F. provided MPI cells and helped with reagents and data generation for macrophages. V.S. performed BioID2 proteomics analysis. B.L. suggested experiments, analyzed the data, and revised the manuscript.

(D and E) Nigericin promotes ASC recruitment by pd-PBs. BMDMs were treated with Ctrl or LPS (L)+nigericin (N). Cells were stained with anti-p62 and anti-EDC4s (D). MPI cells were treated with Ctrl, LPS, H_2O_2, LPS+H_2O_2 (H), LPS+nigericin, or LPS+H_2O_2+nigericin as indicated. The cells were stained with anti-p62, anti-EDC4, and anti-ASC. The percentage of ASC recruited into pd-PBs was quantified by the ASC level versus the p62 level of a droplet. n = 6–11 as indicated (E). Confocal images were acquired.

Scale bars, 10 μm and 2 μm (magnification) (A, B, D, and E). Statistical analysis was performed by one-way ANOVA with Bonferroni multiple-comparisons test. Data are shown as mean ± SEM. The F/degree of freedom/post hoc p values are indicated. **p = 0.0002 (E), ***p < 0.0001 (B and E).

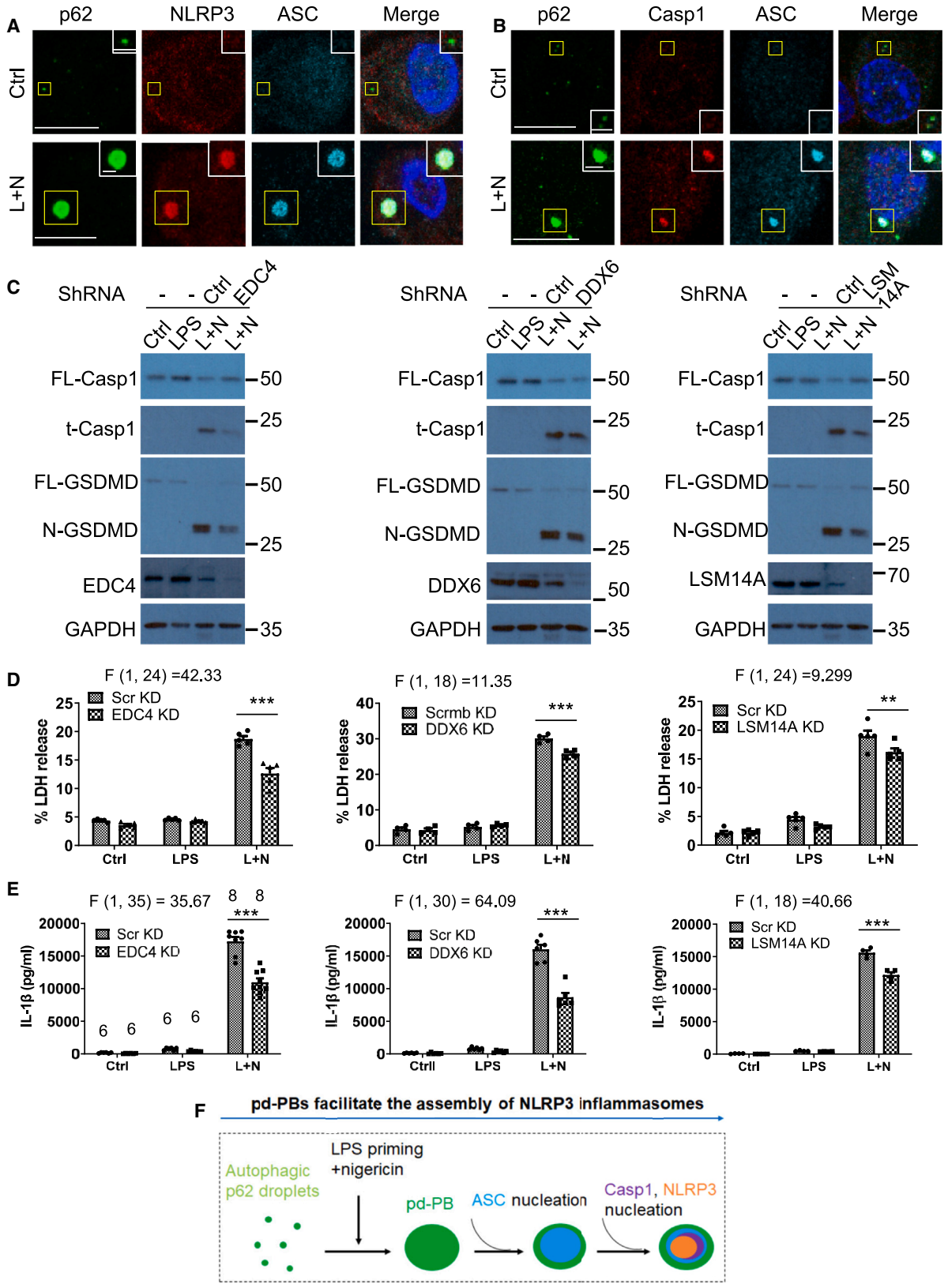

(legend on next page)

DECLARATION OF INTERESTS

The authors declare no competing interests.

Received: August 9, 2023
Revised: January 22, 2024
Accepted: February 22, 2024
Published: March 7, 2024

REFERENCES

1. Pankiv, S., Clausen, T.H., Lamark, T., Brech, A., Bruun, J.A., Outzen, H., Øvervatn, A., Bjørkøy, G., and Johansen, T. (2007). p62/SQSTM1 binds directly to Atg8/LC3 to facilitate degradation of ubiquitinated protein aggregates by autophagy. J. Biol. Chem. *282*, 24131–24145. https://doi.org/10.1074/jbc.M702824200.
2. Sun, D., Wu, R., Zheng, J., Li, P., and Yu, L. (2018). Polyubiquitin chain-induced p62 phase separation drives autophagic cargo segregation. Cell Res. *28*, 405–415. https://doi.org/10.1038/s41422-018-0017-7.
3. Zaffagnini, G., Savova, A., Danieli, A., Romanov, J., Tremel, S., Ebner, M., Peterbauer, T., Sztacho, M., Trapannone, R., Tarafder, A.K., et al. (2018). p62 filaments capture and present ubiquitinated cargos for autophagy. EMBO J. *37*, e98308. https://doi.org/10.15252/embj.201798308.
4. Yang, Y., Willis, T.L., Button, R.W., Strang, C.J., Fu, Y., Wen, X., Grayson, P.R.C., Evans, T., Sipthorpe, R.J., Roberts, S.L., et al. (2019). Cytoplasmic DAXX drives SQSTM1/p62 phase condensation to activate Nrf2-mediated stress response. Nat. Commun. *10*, 3759. https://doi.org/10.1038/s41467-019-11671-2.
5. Parker, R., and Sheth, U. (2007). P bodies and the control of mRNA translation and degradation. Mol. Cell *25*, 635–646. https://doi.org/10.1016/j.molcel.2007.02.011.
6. Wolozin, B., and Ivanov, P. (2019). Stress granules and neurodegeneration. Nat. Rev. Neurosci. *20*, 649–666. https://doi.org/10.1038/s41583-019-0222-5.
7. Protter, D.S.W., and Parker, R. (2016). Principles and Properties of Stress Granules. Trends Cell Biol. *26*, 668–679. https://doi.org/10.1016/j.tcb.2016.05.004.
8. Buchan, J.R., and Parker, R. (2009). Eukaryotic stress granules: the ins and outs of translation. Mol. Cell *36*, 932–941. https://doi.org/10.1016/j.molcel.2009.11.020.
9. Buchan, J.R., Kolaitis, R.M., Taylor, J.P., and Parker, R. (2013). Eukaryotic stress granules are cleared by autophagy and Cdc48/VCP function. Cell *153*, 1461–1474. https://doi.org/10.1016/j.cell.2013.05.037.
10. Lee, K.H., Zhang, P., Kim, H.J., Mitrea, D.M., Sarkar, M., Freibaum, B.D., Cika, J., Coughlin, M., Messing, J., Molliex, A., et al. (2016). C9orf72 Dipeptide Repeats Impair the Assembly, Dynamics, and Function of Membrane-Less Organelles. Cell *167*, 774–788.e17. https://doi.org/10.1016/j.cell.2016.10.002.
11. Molliex, A., Temirov, J., Lee, J., Coughlin, M., Kanagaraj, A.P., Kim, H.J., Mittag, T., and Taylor, J.P. (2015). Phase separation by low complexity domains promotes stress granule assembly and drives pathological fibrillization. Cell *163*, 123–133. https://doi.org/10.1016/j.cell.2015.09.015.
12. Samir, P., Kesavardhana, S., Patmore, D.M., Gingras, S., Malireddi, R.K.S., Karki, R., Guy, C.S., Briard, B., Place, D.E., Bhattacharya, A., et al. (2019). DDX3X acts as a live-or-die checkpoint in stressed cells by regulating NLRP3 inflammasome. Nature *573*, 590–594. https://doi.org/10.1038/s41586-019-1551-2.
13. Braun, J.E., Truffault, V., Boland, A., Huntzinger, E., Chang, C.T., Haas, G., Weichenrieder, O., Coles, M., and Izaurralde, E. (2012). A direct interaction between DCP1 and XRN1 couples mRNA decapping to 5' exonucleolytic degradation. Nat. Struct. Mol. Biol. *19*, 1324–1331. https://doi.org/10.1038/nsmb.2413.
14. Sheth, U., and Parker, R. (2003). Decapping and decay of messenger RNA occur in cytoplasmic processing bodies. Science *300*, 805–808. https://doi.org/10.1126/science.1082320.
15. Hubstenberger, A., Courel, M., Bénard, M., Souquere, S., Ernoult-Lange, M., Chouaib, R., Yi, Z., Morlot, J.B., Munier, A., Fradet, M., et al. (2017). P-Body Purification Reveals the Condensation of Repressed mRNA Regulons. Mol. Cell *68*, 144–157.e5. https://doi.org/10.1016/j.molcel.2017.09.003.
16. Panas, M.D., Ivanov, P., and Anderson, P. (2016). Mechanistic insights into mammalian stress granule dynamics. J. Cell Biol. *215*, 313–323. https://doi.org/10.1083/jcb.201609081.
17. Kedersha, N., Panas, M.D., Achorn, C.A., Lyons, S., Tisdale, S., Hickman, T., Thomas, M., Lieberman, J., McInerney, G.M., Ivanov, P., and Anderson, P. (2016). G3BP-Caprin1-USP10 complexes mediate stress granule condensation and associate with 40S subunits. J. Cell Biol. *212*, 845–860. https://doi.org/10.1083/jcb.201508028.
18. Ohn, T., Kedersha, N., Hickman, T., Tisdale, S., and Anderson, P. (2008). A functional RNAi screen links O-GlcNAc modification of ribosomal proteins to stress granule and processing body assembly. Nat. Cell Biol. *10*, 1224–1231. https://doi.org/10.1038/ncb1783.
19. Kedersha, N., Stoecklin, G., Ayodele, M., Yacono, P., Lykke-Andersen, J., Fritzler, M.J., Scheuner, D., Kaufman, R.J., Golan, D.E., and Anderson, P. (2005). Stress granules and processing bodies are dynamically linked sites of mRNP remodeling. J. Cell Biol. *169*, 871–884. https://doi.org/10.1083/jcb.200502088.
20. Gilks, N., Kedersha, N., Ayodele, M., Shen, L., Stoecklin, G., Dember, L.M., and Anderson, P. (2004). Stress granule assembly is mediated by prion-like aggregation of TIA-1. Mol. Biol. Cell *15*, 5383–5398. https://doi.org/10.1091/mbc.e04-08-0715.
21. Yang, P., Mathieu, C., Kolaitis, R.M., Zhang, P., Messing, J., Yurtsever, U., Yang, Z., Wu, J., Li, Y., Pan, Q., et al. (2020). G3BP1 Is a Tunable Switch that Triggers Phase Separation to Assemble Stress Granules. Cell *181*, 325–345.e28. https://doi.org/10.1016/j.cell.2020.03.046.
22. Youn, J.Y., Dunham, W.H., Hong, S.J., Knight, J.D.R., Bashkurov, M., Chen, G.I., Bagci, H., Rathod, B., MacLeod, G., Eng, S.W.M., et al. (2018). High-Density Proximity Mapping Reveals the Subcellular Organization of mRNA-Associated Granules and Bodies. Mol. Cell *69*, 517–532.e11, e511. https://doi.org/10.1016/j.molcel.2017.12.020.
23. Markmiller, S., Soltanieh, S., Server, K.L., Mak, R., Jin, W., Fang, M.Y., Luo, E.C., Krach, F., Yang, D., Sen, A., et al. (2018). Context-Dependent and Disease-Specific Diversity in Protein Interactions within Stress Granules. Cell *172*, 590–604.e13. https://doi.org/10.1016/j.cell.2017.12.032.

Figure 7. pd-PBs promote NLRP3 inflammasome activation

(A and B) MPI cells were treated as indicated. The cells were stained with anti-p62, anti-ASC, and anti-NLRP3 (A) or with anti-p62, anti-ASC, and anti-C terminus caspase-1 (B). Scale bars, 10 μm and 2 μm (magnification).

(C–E) EDC4, LSM14A, or DDX6 knockdown ameliorates LPS+nigericin-induced inflammation toxicity. MPI cells were treated with Ctrl, LPS, or LPS+nigericin with Ctrl knockdown or EDC4 knockdown (left), with Ctrl knockdown or DDX6 knockdown (center), or with Ctrl knockdown or LSM14A knockdown (right), as indicated. The cell lysates were subjected to western blotting with anti-caspase-1, anti-cleaved GSDMD, anti-EDC4 (or LSM14A, DDX6), and anti-GAPDH successively (C). LDH toxicity was assayed. n = 5 (left and right) and 4 (center) wells (D). IL-1β production was measured by ELISA. n = 6 or 8 wells, as indicated (left), n = 6 wells (center), or n = 4 wells (right) (E). Statistical analysis was performed by two-way ANOVA with Bonferroni multiple-comparisons test. Data are shown as mean ± SEM. The F/degree of freedom/post hoc p values are indicated. $^{**}p < 0.01$, $^{***}p < 0.0001$ (D and E).

(F) The schematic shows that pd-PBs facilitate the assembly of NLRP3 inflammasomes.

24. Gwon, Y., Maxwell, B.A., Kolaitis, R.M., Zhang, P., Kim, H.J., and Taylor, J.P. (2021). Ubiquitination of G3BP1 mediates stress granule disassembly in a context-specific manner. Science *372*, eabf6548. https://doi.org/10.1126/science.abf6548.

25. Li, Y.R., King, O.D., Shorter, J., and Gitler, A.D. (2013). Stress granules as crucibles of ALS pathogenesis. J. Cell Biol. *201*, 361–372. https://doi.org/10.1083/jcb.201302044.

26. Sreedharan, J., Blair, I.P., Tripathi, V.B., Hu, X., Vance, C., Rogelj, B., Ackerley, S., Durnall, J.C., Williams, K.L., Buratti, E., et al. (2008). TDP-43 mutations in familial and sporadic amyotrophic lateral sclerosis. Science *319*, 1668–1672. https://doi.org/10.1126/science.1154584.

27. Kwiatkowski, T.J., Jr., Bosco, D.A., Leclerc, A.L., Tamrazian, E., Vanderburg, C.R., Russ, C., Davis, A., Gilchrist, J., Kasarskis, E.J., Munsat, T., et al. (2009). Mutations in the FUS/TLS gene on chromosome 16 cause familial amyotrophic lateral sclerosis. Science *323*, 1205–1208. https://doi.org/10.1126/science.1166066.

28. Elden, A.C., Kim, H.J., Hart, M.P., Chen-Plotkin, A.S., Johnson, B.S., Fang, X., Armakola, M., Geser, F., Greene, R., Lu, M.M., et al. (2010). Ataxin-2 intermediate-length polyglutamine expansions are associated with increased risk for ALS. Nature *466*, 1069–1075. https://doi.org/10.1038/nature09320.

29. Neumann, M., Sampathu, D.M., Kwong, L.K., Truax, A.C., Micsenyi, M.C., Chou, T.T., Bruce, J., Schuck, T., Grossman, M., Clark, C.M., et al. (2006). Ubiquitinated TDP-43 in frontotemporal lobar degeneration and amyotrophic lateral sclerosis. Science *314*, 130–133. https://doi.org/10.1126/science.1134108.

30. Mackenzie, I.R., Nicholson, A.M., Sarkar, M., Messing, J., Purice, M.D., Pottier, C., Annu, K., Baker, M., Perkerson, R.B., Kurti, A., et al. (2017). TIA1 Mutations in Amyotrophic Lateral Sclerosis and Frontotemporal Dementia Promote Phase Separation and Alter Stress Granule Dynamics. Neuron *95*, 808–816.e9, e809. https://doi.org/10.1016/j.neuron.2017.07.025.

31. Kim, H.J., Kim, N.C., Wang, Y.D., Scarborough, E.A., Moore, J., Diaz, Z., MacLea, K.S., Freibaum, B., Li, S., Molliex, A., et al. (2013). Mutations in prion-like domains in hnRNPA2B1 and hnRNPA1 cause multisystem proteinopathy and ALS. Nature *495*, 467–473. https://doi.org/10.1038/nature11922.

32. Zhou, X., Sumrow, L., Tashiro, K., Sutherland, L., Liu, D., Qin, T., Kato, M., Liszczak, G., and McKnight, S.L. (2022). Mutations linked to neurological disease enhance self-association of low-complexity protein sequences. Science *377*, eabn5582. https://doi.org/10.1126/science.abn5582.

33. Pan, Y., Lu, J., Feng, X., Lu, S., Yang, Y., Yang, G., Tan, S., Wang, L., Li, P., Luo, S., and Lu, B. (2023). Gelation of cytoplasmic expanded CAG RNA repeats suppresses global protein synthesis. Nat. Chem. Biol. *19*, 1372–1383. https://doi.org/10.1038/s41589-023-01384-5.

34. van der Zee, J., Van Langenhove, T., Kovacs, G.G., Dillen, L., Deschamps, W., Engelborghs, S., Matěj, R., Vandenbulcke, M., Sieben, A., Dermaut, B., et al. (2014). Rare mutations in SQSTM1 modify susceptibility to frontotemporal lobar degeneration. Acta Neuropathol. *128*, 397–410. https://doi.org/10.1007/s00401-014-1298-7.

35. Martinon, F., Burns, K., and Tschopp, J. (2002). The inflammasome: a molecular platform triggering activation of inflammatory caspases and processing of proIL-beta. Mol. Cell *10*, 417–426. https://doi.org/10.1016/s1097-2765(02)00599-3.

36. Sharma, D., and Kanneganti, T.D. (2016). The cell biology of inflammasomes: Mechanisms of inflammasome activation and regulation. J. Cell Biol. *213*, 617–629. https://doi.org/10.1083/jcb.201602089.

37. Blobel, G. (1971). Release, identification, and isolation of messenger RNA from mammalian ribosomes. Proc. Natl. Acad. Sci. USA *68*, 832–835.

38. Salomons, F.A., Menéndez-Benito, V., Böttcher, C., McCray, B.A., Taylor, J.P., and Dantuma, N.P. (2009). Selective accumulation of aggregation-prone proteasome substrates in response to proteotoxic stress. Mol. Cell Biol. *29*, 1774–1785. https://doi.org/10.1128/MCB.01485-08.

39. Riggs, C.L., Kedersha, N., Ivanov, P., and Anderson, P. (2020). Mammalian stress granules and P bodies at a glance. J. Cell Sci. *133*, jcs242487. https://doi.org/10.1242/jcs.242487.

40. Vadlamudi, R.K., Joung, I., Strominger, J.L., and Shin, J. (1996). p62, a phosphotyrosine-independent ligand of the SH2 domain of p56lck, belongs to a new class of ubiquitin-binding proteins. J. Biol. Chem. *271*, 20235–20237.

41. Hofmann, S., Kedersha, N., Anderson, P., and Ivanov, P. (2021). Molecular mechanisms of stress granule assembly and disassembly. Biochim. Biophys. Acta. Mol. Cell Res. *1868*, 118876. https://doi.org/10.1016/j.bbamcr.2020.118876.

42. Kedersha, N., Cho, M.R., Li, W., Yacono, P.W., Chen, S., Gilks, N., Golan, D.E., and Anderson, P. (2000). Dynamic shuttling of TIA-1 accompanies the recruitment of mRNA to mammalian stress granules. J. Cell Biol. *151*, 1257–1268. https://doi.org/10.1083/jcb.151.6.1257.

43. Ravikumar, B., Vacher, C., Berger, Z., Davies, J.E., Luo, S., Oroz, L.G., Scaravilli, F., Easton, D.F., Duden, R., O'Kane, C.J., and Rubinsztein, D.C. (2004). Inhibition of mTOR induces autophagy and reduces toxicity of polyglutamine expansions in fly and mouse models of Huntington disease. Nat. Genet. *36*, 585–595. https://doi.org/10.1038/ng1362.

44. Fejer, G., Wegner, M.D., György, I., Cohen, I., Engelhard, P., Voronov, E., Manke, T., Ruzsics, Z., Dölken, L., Prazeres da Costa, O., et al. (2013). Nontransformed, GM-CSF-dependent macrophage lines are a unique model to study tissue macrophage functions. Proc. Natl. Acad. Sci. USA *110*, E2191–E2198. https://doi.org/10.1073/pnas.1302877110.

45. Fitzgerald, K.A., Rowe, D.C., Barnes, B.J., Caffrey, D.R., Visintin, A., Latz, E., Monks, B., Pitha, P.M., and Golenbock, D.T. (2003). LPS-TLR4 signaling to IRF-3/7 and NF-kappaB involves the toll adapters TRAM and TRIF. J. Exp. Med. *198*, 1043–1055. https://doi.org/10.1084/jem.20031023.

46. Zhong, Z., Umemura, A., Sanchez-Lopez, E., Liang, S., Shalapour, S., Wong, J., He, F., Boassa, D., Perkins, G., Ali, S.R., et al. (2016). NF-kappaB Restricts Inflammasome Activation via Elimination of Damaged Mitochondria. Cell *164*, 896–910. https://doi.org/10.1016/j.cell.2015.12.057.

47. Yu, J.H., Yang, W.H., Gulick, T., Bloch, K.D., and Bloch, D.B. (2005). Ge-1 is a central component of the mammalian cytoplasmic mRNA processing body. RNA *11*, 1795–1802. https://doi.org/10.1261/rna.2142405.

48. Yang, W.H., Yu, J.H., Gulick, T., Bloch, K.D., and Bloch, D.B. (2006). RNA-associated protein 55 (RAP55) localizes to mRNA processing bodies and stress granules. RNA *12*, 547–554. https://doi.org/10.1261/rna.2302706.

49. Andrei, M.A., Ingelfinger, D., Heintzmann, R., Achsel, T., Rivera-Pomar, R., and Lührmann, R. (2005). A role for eIF4E and eIF4E-transporter in targeting mRNPs to mammalian processing bodies. RNA *11*, 717–727. https://doi.org/10.1261/rna.2340405.

50. Ayache, J., Bénard, M., Ernoult-Lange, M., Minshall, N., Standart, N., Kress, M., and Weil, D. (2015). P-body assembly requires DDX6 repression complexes rather than decay or Ataxin2/2L complexes. Mol. Biol. Cell *26*, 2579–2595. https://doi.org/10.1091/mbc.E15-03-0136.

51. Lamark, T., Perander, M., Outzen, H., Kristiansen, K., Øvervatn, A., Michaelsen, E., Bjørkøy, G., and Johansen, T. (2003). Interaction codes within the family of mammalian Phox and Bem1p domain-containing proteins. J. Biol. Chem. *278*, 34568–34581. https://doi.org/10.1074/jbc.M303221200.

52. Wilson, M.I., Gill, D.J., Perisic, O., Quinn, M.T., and Williams, R.L. (2003). PB1 domain-mediated heterodimerization in NADPH oxidase and signaling complexes of atypical protein kinase C with Par6 and p62. Mol. Cell *12*, 39–50. https://doi.org/10.1016/s1097-2765(03)00246-6.

53. Valionyte, E., Yang, Y., Griffiths, S.A., Bone, A.T., Barrow, E.R., Sharma, V., Lu, B., and Luo, S. (2022). The caspase-6-p62 axis modulates p62 droplets based autophagy in a dominant-negative manner. Cell Death Differ. *29*, 1211–1227. https://doi.org/10.1038/s41418-021-00912-x.

54. Sha, Z., Blyszcz, T., González-Prieto, R., Vertegaal, A.C.O., and Goldberg, A.L. (2019). Inhibiting ubiquitination causes an accumulation of

SUMOylated newly synthesized nuclear proteins at PML bodies. J. Biol. Chem. *294*, 15218–15234. https://doi.org/10.1074/jbc.RA119.009147.

55. Hyer, M.L., Milhollen, M.A., Ciavarri, J., Fleming, P., Traore, T., Sappal, D., Huck, J., Shi, J., Gavin, J., Brownell, J., et al. (2018). A small-molecule inhibitor of the ubiquitin activating enzyme for cancer treatment. Nat. Med. *24*, 186–193. https://doi.org/10.1038/nm.4474.
56. Cavey, J.R., Ralston, S.H., Hocking, L.J., Sheppard, P.W., Ciani, B., Searle, M.S., and Layfield, R. (2005). Loss of ubiquitin-binding associated with Paget's disease of bone p62 (SQSTM1) mutations. J. Bone Miner. Res. *20*, 619–624. https://doi.org/10.1359/JBMR.041205.
57. Hondele, M., Sachdev, R., Heinrich, S., Wang, J., Vallotton, P., Fontoura, B.M.A., and Weis, K. (2019). DEAD-box ATPases are global regulators of phase-separated organelles. Nature *573*, 144–148. https://doi.org/10.1038/s41586-019-1502-y.
58. He, Y., Hara, H., and Núñez, G. (2016). Mechanism and Regulation of NLRP3 Inflammasome Activation. Trends Biochem. Sci. *41*, 1012–1021. https://doi.org/10.1016/j.tibs.2016.09.002.
59. Komatsu, M., Kurokawa, H., Waguri, S., Taguchi, K., Kobayashi, A., Ichimura, Y., Sou, Y.S., Ueno, I., Sakamoto, A., Tong, K.I., et al. (2010). The selective autophagy substrate p62 activates the stress responsive transcription factor Nrf2 through inactivation of Keap1. Nat. Cell Biol. *12*, 213–223. https://doi.org/10.1038/ncb2021.
60. Ohnishi, T., Bandow, K., Kakimoto, K., Kusuyama, J., and Matsuguchi, T. (2014). Long-time treatment by low-dose N-acetyl-L-cysteine enhances proinflammatory cytokine expressions in LPS-stimulated macrophages. PLoS One *9*, e87229. https://doi.org/10.1371/journal.pone.0087229.
61. Danieli, A., Vucak, G., Baccarini, M., and Martens, S. (2023). Sequestration of translation initiation factors in p62 condensates. Cell Rep. *42*, 113583. https://doi.org/10.1016/j.celrep.2023.113583.
62. Currais, A., Fischer, W., Maher, P., and Schubert, D. (2017). Intraneuronal protein aggregation as a trigger for inflammation and neurodegeneration in the aging brain. Faseb. J. *31*, 5–10. https://doi.org/10.1096/fj.201601184.
63. Swinnen, B., Robberecht, W., and Van Den Bosch, L. (2020). RNA toxicity in non-coding repeat expansion disorders. EMBO J. *39*, e101112. https://doi.org/10.15252/embj.2018101112.
64. Ichimura, Y., Waguri, S., Sou, Y.S., Kageyama, S., Hasegawa, J., Ishimura, R., Saito, T., Yang, Y., Kouno, T., Fukutomi, T., et al. (2013). Phosphorylation of p62 activates the Keap1-Nrf2 pathway during selective autophagy. Mol. Cell *51*, 618–631. https://doi.org/10.1016/j.molcel.2013.08.003.
65. Yamamoto, A., Cremona, M.L., and Rothman, J.E. (2006). Autophagy-mediated clearance of huntingtin aggregates triggered by the insulin-signaling pathway. J. Cell Biol. *172*, 719–731. https://doi.org/10.1083/jcb.200510065.
66. Kim, D.I., Jensen, S.C., Noble, K.A., Kc, B., Roux, K.H., Motamedchaboki, K., and Roux, K.J. (2016). An improved smaller biotin ligase for BioID proximity labeling. Mol. Biol. Cell *27*, 1188–1196. https://doi.org/10.1091/mbc.E15-12-0844.
67. Roux, K.J., Kim, D.I., and Burke, B. (2013). BioID: a screen for protein-protein interactions. Curr. Protoc. Protein Sci. *74*, 19.23.1–19.23.14. https://doi.org/10.1002/0471140864.ps1923s74.

STAR★METHODS

KEY RESOURCES TABLE

REAGENT or RESOURCE	SOURCE	IDENTIFIER
Antibodies		
Anti-p62	MBL	Cat# PM045; RRID:AB_1279301
Anti-Flag	Cell Signaling Technology	Cat# 14793; RRID:AB_2572291
Anti-GFP	Cell Signaling Technology	Cat# 2956; RRID:AB_1196615
Anti-Myc	Cell Signaling Technology	Cat# 2272; RRID:AB_10692100
Anti-EDC4	Cell Signaling Technology	Cat #2548; RRID:AB_10621246
Anti-eIF4E	Cell Signaling Technology	Cat# 9742; RRID:AB_823488
Anti-4EBP	Cell Signaling Technology	Cat# 2855; RRID:AB_560835
Anti-G3BP2	Cell Signaling Technology	Cat# 31799; RRID:AB_2920540
Anti-ASC	Cell Signaling Technology	Cat# 67824; RRID:AB_2799736
Anti-ubiquitin (P4D1)	Cell Signaling Technology	Cat# 3936; RRID:AB_331292
Anti-mTOR	Cell Signaling Technology	Cat# 5536; RRID:AB_10691552
Anti-caprin1	Proteintech	Cat# 15112-1-AP; RRID:AB_2070016
Anti-TFEB	Proteintech	Cat# 13372-1; RRID:AB_2199611
Anti-GAPDH	Ambion	Cat# AM4300; RRID:AB_437392
Anti-HA	Biolegend	Cat# 901501; RRID:AB_2565006
Anti-EF-2/eEF2 (C-9)	Santa Cruz	Cat# sc-166415; RRID:AB_2277758
Anti-EDC4 (H-12)	Santa Cruz	Cat# sc-376382; RRID:AB_10988077
Anti-GW182 (4B6)	Santa Cruz	Cat# sc-56314; RRID:AB_783673
Anti-Dcp1a (56-Y)	Santa Cruz	Cat# sc-100706; RRID:AB_2090408
Anti-RCK/DDX6 (E−12)	Santa Cruz	Cat# sc-376433; RRID:AB_11151042
Anti-RAP55/LSM14A (C-5)	Santa Cruz	Cat# sc-398552
Anti-G3BP1	Santa Cruz	Cat# sc-81940; RRID:AB_1123055
Anti-YTHDF3 (F-2)	Santa Cruz	Cat# sc-377119; RRID:AB_2687436
Anti-LIMP2	Invitrogen	Cat# PAS-20540; RRID:AB_11156197
Anti-p62 (C terminus)	Progen	Cat# GP62-C; RRID:AB_2687531
Anti-Caspase-1	Santa Cruz	Cat# 14F468; RRID:AB_781816
Anti-GSDMD	Abcam	Cat# ab209845; RRID:AB_2783550
Anti-NLRP3 (Cryo-2)	Adipogen	Cat# AG-20B-0014; RRID:AB_2490202
Anti-IL-1β	ThermoFisher Scientific	Cat# 14701285; RRID:AB_468397
Anti-Flag (M2) agarose affinity gel	Sigma-Aldrich	Cat# A2220; RRID:AB_10063035
Anti-HA agarose	Sigma-Aldrich	Cat# A2095; RRID:AB_257974
Secondary antibodies for EM: 18 nm colloidal gold, goat anti-rabbit	Jackson ImmunoResearch	Cat# 111-215-144; RRID:AB_2338017
10 nm gold, goat anti-mouse	Merck	Cat# G7652; RRID:AB_259958
Chemicals, peptides, and recombinant proteins		
PI-103	Calbiochem	#528100
Staurasporine	Merck	#S5921
Hygromycin B	Merck	#H3274
G418	Thermo Fisher	#11811023
Puromycin	Santa Cruz	#53-79-2
MG-132	Merck	#M8699
Etoposide	Merck	#E1383

(*Continued on next page*)

Continued

REAGENT or RESOURCE	SOURCE	IDENTIFIER
cycloheximide	Merck	#C4859
LPS	Sigma-Aldrich	#L7261
Nigericin	Bio-Techne	#4312/10
H2O2	Fluka	#31641
Doxycycline Hydrochloride	Fisher Bioreagents	#10592-12-9
Sodium arsenite	Merck	#1062771000
Sorbitol	Fisher Scientific	#BP439-500
TAK-243	MCE	#HY-100487
N-Acetyl-cysteine (NAC)	Sigma-Aldrich	#A7250
Biotin	Fisher Scientific	#BP232-1
Critical commercial assays		
CyQUANT LDH Cytotoxicity Assay	ThermoFisher Scientific	C20302
Deposited data		
Raw proteomics data (Table S1)	This paper	PRIDE partner repository, data identifier PXD049350
Raw proteomics data (Table S2)	This paper	PRIDE partner repository, data identifier PXD049396
Experimental models: Cell lines		
HeLa cells	ATCC	#CCL-2
p62 WT MEFs	Ichimura et al.[64]	N/A
p62 KO MEFs	Ichimura et al.[64]	N/A
p62 WT HAP1 cells	Yang et al.[4]	N/A
p62 KO HAP1 cells	Yang et al.[4]	N/A
Tet-off CFP-HTT-exon1-103Q HeLa cells	Yamamoto et al.[65]	N/A
MPI macrophages	Fejer et al.[44]	N/A
Primary BMDMs	This paper	N/A
HEK293T	ECACC	12022001
x-63 cells	Fejer et al.[44]	N/A
Oligonucleotides		
Oligonucleotides for cDNA cloning	This paper	Table S3
Oligonucleotides for siRNAs	This paper	Table S3
Recombinant DNA		
Mouse p62 shRNA	Sigma-Aldrich	TRCN0000238135
Mouse EDC4 shRNA	Sigma-Aldrich	TRCN0000243536
Mouse LSM14A shRNA	Sigma-Aldrich	TRCN0000177282
Mouse DDX6 shRNA	Sigma-Aldrich	TRCN0000103600
Mouse ASC/PYCARD shRNA	Sigma-Aldrich	TRCN0000087114
MCS-BioID2-HA	Kim et al.[66]	Addgene #74224
pcDNA3.1-DDX6	GeneScript	#OHu14789D
pEGFP-C1-p62	Yang et al.[4]	Table S4
pEGFP-C1-p62-N (1–256)	Valionyte et al.[53]	Table S4
pCMV-6M-p62	Valionyte et al.[53]	Table S4
pET28a-p62	Yang et al.[4]	Table S4
MCS-BioID2-p62-HA	This paper	Table S4
pcCMV5c-p62-Flag	This paper	Table S4
pHA-C1-p62	This paper	Table S4
pLJM1-EGFP-p62	This paper	Table S4
pGEX-6P-1-p62	This paper	Table S4

(*Continued on next page*)

Continued

REAGENT or RESOURCE	SOURCE	IDENTIFIER
pEGFP-C1-DDX6	This paper	Table S4
pET28a-GFP-DDX6	This paper	Table S4
Software and algorithms		
Prism GraphPad 9.5.1	https://www.graphpad.com	https://www.graphpad.com
ImageJ v1.41	NIH	https://ImageJ.net/ij/index.html; RRID: SCR_003070

RESOURCE AVAILABILITY

Lead contact

Further information and requests for reagents should be directed to the lead contact, Shouqing Luo (shouqing.luo@plymouth.ac.uk).

Materials availability

Materials generated in this study will be available upon request.

Data and code availability

- The mass spectrometry proteomics data have been deposited to the ProteomeXchange Consortium via the PRIDE partner repository (PRIDE: PXD049350, PXD049396).
- This paper does not report original code.
- Any additional information required to re-analyze the data reported in this paper is available from the lead contact upon request.

EXPERIMENTAL MODEL AND SUBJECT PARTICIPANT DETAILS

Culture of cell lines

HeLa cells were cultured with standard methods in Dulbecco's Modified Eagle's Medium (DMEM) (Merck, D6429) supplemented with 10% (v/v) fetal bovine serum (FBS) (Gibco, 10500-064) and 1/100 (v/v) 100 × penicillin-streptomycin-L-glutamine (ThermoFisher, #10378016) (full DMEM media). p62 KO MEFs and WT MEFs (provided by Dr M. Komatsu) were also cultured in full DMEM media. p62 KO or WT HAP1 cells were cultured in Iscove's Modified Dulbecco's Medium (IMDM), supplemented with 10% FBS (Gibco, 10500-064). Stably Tet-off CFP-HTT-exon1-103Q expressing HeLa cells (offered by A. Yamamoto) were cultured in DMEM supplemented with 10% FBS containing 100 μg/mL G148 and 50 μg/mL Hygromycin B. The removal of expressed CFP-HTT-103Q was induced with 250 ng/mL doxycycline. MPI macrophages were cultured in RPMI 1640 media (Merck, R0883) supplemented with 10% (v/v) FBS, 1% (v/v) 100 × penicillin-streptomycin-L-glutamine and 1% (v/v) GM-CSF condition medium produced by X-63 cells. To passage cells, suspended cells were removed and PBS-EDTA (Lonza Bioscience, BE02-017F) was used to dissociate adhered cells. Subsequently, cells were centrifuged at 600 × g for 3 min and resuspended in fresh media, supplemented with GM-CSF condition medium. Cells were passaged twice weekly and cultured up to passage 20. To generate GM-CSF condition medium, X-63 cells were cultured in RPMI 1640 media supplemented with 10% (v/v) FBS and % (v/v) 100 × penicillin-streptomycin-L-glutamine for 7 days. Media were collected, filtered using 0.22 μm syringe filter and stored in −80°C until use.

Culture of primary BMDMs

Bone marrows were harvested from 6 to 8 week-old C57/B6/J male mice. The mice were sacrificed according to the rules and regulations by University of Plymouth and the Home Office. All work was completed in a tissue culture hood. Briefly, the femurs and tibias of the hind legs were obtained without breaking and kept in ice-cold PBS during the procedure. Soft tissues were removed from the bones, which were sterilized in 70% ethanol for 5 min and washed with sterile PBS. Bones were cut at both ends and flushed with sterile PBS using 25-gauge needle to expel the bone marrow. Cells were centrifuged for 5 min at 500 × g, and pellets were resuspended in DMEM supplemented with 20% FBS, 1 mM sodium pyruvate, 1 mM glutamine, 100 U/ml penicillin/streptomycin. Cells were counted using hemocytometer. Each well of a 6-well plate was seeded with a million cells, topped with 3 mL complete BMDM media and supplemented with 30 ng/mL recombinant murine M-CSF (Peprotech, 315-02). On day 3, 3 mL complete BMDM media were added to each well to replenish the nutrients. On day 7, BMDMs were fully differentiated and attached. Cells were washed with PBS to remove residual red blood cells, supplemented with fresh media and subjected to treatments according to experimental plan.

All cells were maintained at 37 °C at a 5% CO_2 level. Authentication was confirmed by the suppliers, and by morphology check with light microscopy. All the cell lines used were negative for mycoplasma.

METHOD DETAILS

Drug treatment

To induce proteotoxicity, cells were treated with puromycin for 3.5 h at a final concentration of 10 μg/mL (for HeLa cells and MEFs), or 2 μg/mL (for HAP1 cells). MG-132 (5 μM) was used for 5-h treatment. Cells were treated with cycloheximide (50 μg/mL) for 3.5 h. For TAK-243 treatment, cells were incubated with TAK-243 at a final concentration of 1 μM overnight. Cells were treated with H2O2 (200 μM) for 24 h. Nigericin (20 μM) alone was used for 2-h treatment. LPS (100 ng/mL) was added to cells for 24-h treatment. For LPS + nigericin treatment, cells were treated with LPS (100 ng/mL) for 24 h and nigericin (20 μM) for 2 h. For NAC treatment, cells were pre-treated with NAC (200 μM or 20 mM, as indicated in the figure legend) for 2 h, and NAC was present in the time course of LPS + nigericin treatment.

DNA cloning and mutagenesis

Plasmids for p62 point mutants, pEGFP-C1-p62-M404V, pEGFP-C1-p62-N (1-256aa) were generated using the Quikchange Multi Site-directed Mutagenesis kit according to manufacturing instruction (Agilent Technologies, #200514). Mutations were confirmed by DNA sequencing. Oligonucleotides for DNA cloning and mutagenesis can be found in Table S3. The cloning methods for the plasmids used in this study are shown in Table S4.

siRNAs

The siRNAs used are listed with their sources and sequences in Table S3.

DNA and siRNA transfection

Cells were split 1 day prior to transfection to 50–80% confluency and left overnight in DMEM containing 10% FBS. DNA constructs and siRNAs were generally transfected with Lipofectamine 2000 according to the manufacturer's instructions. For each well of the 6-well plate, 100 μL Opti-MEM containing transfected plasmids was mixed with 100 μL Opti-MEM with lipofectamine. After 15-min incubation, the transfection mixture was added to the cells, where the medium was pre-changed with 0.8 mL of antibiotics-free DMEM containing 10% FBS. For DNA transfection, 0.1–0.3 μg of each plasmid was used for a well of a 6-well plate, or the proportional amount of plasmids was transfected for a well of a non-6-well plate. 2 μL of Lipofectamine 2000 reagent (Invitrogen, #52887) was used for each μg plasmid DNA. Media containing the transfection reagent was changed with full DMEM media 4 h after transfection. Transfected cells were typically harvested or fixed 20 h post transfection. For siRNA transfection, siRNAs were transfected at a final concentration of 50 nM, and 1 μL of Lipofectamine 2000 reagent was used for each 20 pmol siRNA. HeLa cells were maintained in 10% FBS DMEM containing no antibiotics for 24 h after transfection. After 24 h, the siRNAs transfected cells were either split for subsequent experiments or were cultured continuously with full DMEM media until harvested or fixed for further analysis.

BioID2

The BioID2 pulldown experiments were performed as previously described.[67] Four 10-cm dishes were used for each experimental condition. 1.2 μg of BioID2-HA empty plasmid or BioID-p62-HA was transfected for each individual plate. Biotin (50 μM) was added at 6-h post transfection. The cells were harvested on the following day. The harvested cells from each dish were lysed in 1-mL Buffer A for 10 min on ice. The samples were centrifuged at 4 °C at 13,000 × g for 10 min. 400 μL of streptavidin magnetic Sepharose beads (Cytiva, #28985738) were equilibrated and added to each falcon tube with the cell supernatant for 3-h incubation at 4°C. The samples were then thoroughly washed 6 times with Buffer A (20 mM Tris-HCl, pH 7.4, 2 mM MgCl2, 150 mM NaCl, 0.5% NP-40, protease inhibitor cocktail (Thermo)). 40 μL of 1 mM biotin was added to each sample to elute BioID2 pulldown products before being stored in the −80 freezer until mass spectrometry analysis was performed.

Liquid chromatography and tandem mass spectrometry

BioID2 pulldown products were digested using sequence specific enzyme trypsin and tandem mass spectrometry experiments were performed on digested and purified peptides using the Ultimate 3000 UPLC system (Thermo Fisher) connected to the Orbitrap Velos Pro mass spectrometer (Thermo Fisher). Data acquisition with the Orbitrap instrument was performed in a data-dependent mode to automatically switch between MS and MS2. Proteins were identified with the Andromeda search engine integrated in the MaxQuant version 1.5.0.30 program. The peak lists were queried against the relevant database downloaded from www.uniprot.org and supplemented with frequently observed contaminants and concatenated with reversed copies of all entries. Andromeda search parameters for protein identification were specified with a false discovery rate of less than 1%. LFQ was used for relative protein quantification. Fisher's exact tests were applied to calculate p values of protein enrichment.

Global protein translation assay

The global translation assay was conducted with the protein synthesis assay kit (Abcam, #ab235634) according to the manufacturer's instruction. Cells were incubated with the protein label (400 ×) for 2 h. Following the appropriate pre-treatment times, samples were incubated with the fixative solution for 15 min at room temperature. The samples were then washed with the wash buffer and incubated in the permealization buffer for 10 min at room temperature. Samples were incubated with the reaction cocktail for 30 min

at room temperature. Cells underwent three 10-min washes in the wash buffer. The samples were then stained for p62. Images were gathered on the confocal microscope with red fluorescence generated by the protein label to show the level of protein translation in individual cells.

Fluorescence recovery after photo bleaching (FRAP)

Live cells were subjected to FRAP analysis using an oil immersion objective (63×). GFP-p62 puncta were bleached for 11.8 s (8 × 1.477s) with an 80% laser intensity of 488 nm. The chamber of the microscope was maintained at 37°C. One image of the selected cell was taken before bleaching. Following this, 50 images of the puncta were taken post-bleaching to visualize fluorescence levels over time. Recovery was recorded by fluorescence intensity for the indicated times.

Immunocytochemistry

Cells were fixed with 4% paraformaldehyde for 10 min. The fixed cells were washed three times in PBS, then permeabilized with PBS containing 0.5% Triton X-100 for 10 min. Cells were blocked in blocking buffer (1% BSA, 1% heat inactivated goat serum in PBS) for 30 min at room temperature. Primary antibodies were diluted and incubated with cells overnight at 4°C. The secondary antibody was incubated for 30 min after washing three times with PBS (10 min, each). Cells were washed with PBS three times (10 min, each) after incubation with secondary antibodies, then mounted with DAPI (1 μg/mL). Images were acquired using a Leica confocal microscope.

Immunogold labeling

Cells were gently harvested using a scrapper and centrifuged for 5 min at 600 × g. The pellets were washed with pre-warmed PBS twice. The cells were subjected to fixation using McDowell Trump's fixative (4% formaldehyde, 0.5% glutaraldehyde, 0.1M PIPES buffer, pH 7.4) for 20 min at room temperature and a minimum of 2 h at 4°C. The pellets were rinsed using 0.1M PIPES buffer (pH 7.4), three times for 15 min. Fixed pellets were subjected to serial alcohol dehydration (50%, 60%, 70% and 80% ethanol) for 10 min each. Gradually, the cells were infiltrated with increasing LR White resin concentration (50%, 70%, 2 × 100% LR White resin in ethanol), overnight per concentration. Each sample was transferred to the beem capsule filled with fresh LR White resin and baked for 24 h at 50°C. Embedded pellets were ultra-sectioned at 100 nm onto gold grids.

Section-containing grids were first washed in 0.05 M glycine in PIPES buffer for 5 min, carefully blotted on the clean tissue to remove the excess glycine and rinsed twice with incubation buffer (1% normal goat serum, 1% BSA, 5% TBST). Grids were subsequently incubated in blocking buffer (3% normal goat serum, 2% BSA, 5% TBST) for 1 h at room temperature. The grids were rinsed with incubation buffer twice for 2 min to remove the excess blocking buffer. The grids were then co-incubated with primary antibodies (mouse anti-HA (1:20) and rabbit anti-Myc (1:20)) for 3 h at room temperature. Grids were washed with incubation buffer three times for 2 min and incubated with secondary antibodies: anti-mouse (10 nm colloidal gold, Merck, #G7652) (1:20) and anti-rabbit (18 nm gold, Jackson ImmunoResearch, #111-215-144) (1:20), for 2 h at room temperature. The grids were then washed with incubation buffer twice for 2 min and with distilled water twice for 2 min, and let dry on tissue paper overnight. Lastly, the sections were subjected to contrast staining using uranyl acetate for 10 min at room temperature, followed by three rinses with distilled water. Transmission electron images were acquired using JEOL 1400 TEM microscope.

RNA Fluorescent *in situ* hybridization (FISH)

Cells underwent immunocytochemistry as previously described. All the reagents used were freshly made and sterile, and during incubations, a RiboLock RNase Inhibitor (ThermoFisher Scientific, EO0381) was added at a 1:100 dilution to prevent RNA degradation. The following steps were undertaken at room temperature unless otherwise specified. Following three 10-min PBS washes after the secondary antibody incubation, samples were post-fixed in 4% PFA and underwent two 5-min washes in 2 × SSC. The hybridization buffer was then made with the reagents listed in the table. The samples were incubated in the hybridization mixture for 18–20 h at 42°C. The samples were then washed three times in 50% formamide in 2 × SSC for 5 min each at 37°C. The samples then underwent three 5-min washes in 2 × SSC and 1 × SSC at 37°C, successively. Finally, samples were washed twice for 10 min in 4 × SSC. The samples were then mounted using a DAPI mounting media (1μg/ml). Images were gathered on a Leica confocal microscope.

Hybridization mixture for a sample (80 μL per coverslip)

Components	For one sample (80 μL required per coverslip)
Formamide	20 μL
20 × SSC	8 μL
tRNA	3.2 μL
50% dextran	16 μL
H_20	32.6 μL
Oligod(dT)30 (1μg/μl)	0.2 μL

Generating lentivirus and transduction

HEK293T cells were transfected with pCMV-VSV.G envelope, psPAX2 packaging and the plasmid of interest at the ratio of 1:3:4. Total of 5 μg DNA was transfected per 6 well using Lipofectamine 3000 (ThermoFisher Scientific, L3000001). 24 h and 48 h-post transfection, the viral media was harvested, filtered using 0.22 μm syringe filter and supplemented with 4 μM Polybrene. MPI cells were transduced at a ratio of 2:1 using lentiviral media and supplemented with 4 μM Polybrene. 72 hour-post transduction, MPI cells were subjected to further treatment and analysis as indicated in each experiment.

Western blot analysis

Cells were lysed in Buffer A (20mM Tris-HCl, pH 7.2, 2mM MgCl2, 150mM NaCl, 0.5% NP-40) with the protease inhibitor (Thermo Scientific/Pierce, #A32953). Protein concentrations were measured with a BCA protein assay kit (Thermo Scientific/Pierce, #23225). Cell lysates or protein solutions were mixed with an equal volume of 2 × Laemmli buffer, and boiled at 100°C for 10 min. The boiled protein samples were subjected to 10% or 12.5% SDS-PAGE resolution, and subsequently transferred to the PVDF membrane (Thermo Scientific, #88518). The PVDF membrane was blocked in 5% (w/v) semi-skimmed milk in 1 × TBS with 0.05% Tween 20 (TBST), and incubated with a primary antibody at 4°C typically overnight in TBST containing 5% milk, followed by three 5-min washes with TBST. The membrane was incubated with a secondary antibody (cross-linked with HRP) at room temperature for 30 min. After three washes (5 min each), protein bands on the membrane were detected with the ECL western blotting substrate (Pierce, #32106 or GE, #RPN2232).

6 × his-tagged protein expression and purification

p62 or GFP-DDX6 was cloned into pET-28a for 6 × His-tagged protein expression. A plasmid was transformed into BL21 (DE3). A final concentration of 0.2 mM IPTG was added to LB broth to induce recombinant protein expression. 6 × His-tagged proteins were purified with Ni^{2+} charged 6 × His-tag affinity resins (Millipore) according to manufacture instruction. 500 mL bacterial LB were centrifuged (5,000 × g, 15 min), and resuspended in 50 mL 1 × Ni-NTA binding buffer (50 mM NaH2PO4 pH 8.0, 300 mM NaCl, 10 mM imidazole) with 5 mL of 10 × BugBuster protein extraction reagent (Millipore), 50 μl benzonase nuclease (250 U/μL) (Thermo, #88701), 50 KU (100 μl, 50 mg/mL) rlysozyme (Thermo, #90082) and 8 tablets of protease inhibitor (Pierce, A32953). The lysates were centrifuged twice with 5,000 × g, 15 min. The supernatant was incubated with 2.4 mL 50% 6 × His-affinity beads (pre-washed with 1 × Ni-NTA binding buffer) for 1 h at room temperature. After the incubation, the beads were extensively washed with 1 × Ni-NTA washing buffer (50 mM NaH2PO4 pH 8.0, 300 mM NaCl, 20 mM imidazole), 4 times (10 mL/time). GFP-DDX6 was eluted with 1.2 mL 1 × Ni-NTA elution buffer (50 mM NaH2PO4 pH 8.0, 300 mM NaCl, 250 mM imidazole) twice. The proteins were subjected to size exclusive chromatography with Superose 6 Increase 10/300 GL (GE Healthcare). The eluates were concentrated, and the elution buffer was exchanged with the desired stock buffer (40 mM Tris, pH 7.4, 1 mM DTT, 10% glycerol) using a 4-mL EMD Amicon Ultra centrifugal filter unit (Millipore). Protein concentration was measured by BCA assays.

Immunoprecipitation

Immunoprecipitation (IP) was performed using Buffer A (20 mM Tris-HCl, pH 7.4, 2 mM MgCl2, 150 mM NaCl, 0.5% NP-40, protease inhibitor cocktail (Thermo)). Cells were lysed in 300–350 μL Buffer A for 15 min on ice, followed by centrifugation at 13,000 × g for 15 min 500 μg - 1 mg total proteins were used as the starting material for immunoprecipitations. An antibody was added to the cell lysate at 1:100 dilution. After a 2-h incubation at 4°C, 20 μL Buffer A pre-washed protein A/G beads were added for a further 30-min incubation at 4°C. The beads were extensively washed by Buffer A. Alternatively, Buffer A pre-washed anti-Flag antibody (M2) or anti-HA agarose affinity gel was added to the protein lysate and incubated for 2 h at 4°C. The agarose gel was washed at least 3 times with Buffer A. Immunoprecipitation products were directly boiled in Laemmli buffer or stored in −80°C for Western blot analysis.

Polyubiquitinated protein purification

HA-ubiquitin plasmid (pcDNA-HA-3 × ubiquitin) was transfected into HeLa cells in 3 × 10-cm dishes. After 20 h, the cells were treated with puromycin (5 μg/μL, 5 h) to enrich HA-polyubiquitinated proteins. HA-polyubiquitinated proteins were subjected to immunoprecipitation with 40 μL anti-HA agarose beads. The pull-down products were eluted with 120 μL of 0.1 M glycine (pH 2.5) by 10-min incubation at room temperature. The eluate was neutralized with 30 μL of 1M Tris-HCl pH 7.4. The purified polyubiquitinated proteins were measured for concentration by BCA assays, and aliquoted for *in vitro* phase separation assays. Protein molar concentration was estimated using the averaged molecular weight of 40 kDa.

In vitro DDX6 phase-separation

GFP-DDX6 *in vitro* droplet phase separation was carried out in a glass-bottomed well of a 384-well plate in the buffer modified from the basal phase separation buffer (BPSB)-based buffer (detailed below). Purified recombinant GFP-DDX6 or p62 was stored in 40 mM Tris-HCl, pH 7.4, 1 mM DTT and 10% glycerol. To optimize the conditions for *in vitro* DDX6 phase separation, phase separation buffer was adjusted from BPSB with modification of pH, polyU or ATP, or salt concentration, as indicated, to assess subsequent conditions of phase separation. Final concentration was 2 μM, 4 μM, or 8 μM. For the role of p62 in DDX6 phase separation,

4 μM GFP-DDX6 in the presence or the absence of p62 and/or poly-ubiquitin chains (poly-Ub), was phase-separated in BPSB without ATP. In the case of GFP-DDX6 only, the following recipe was used:

(1 × BPSB, ATP-) buffer: 4.2 μL.
50 μM GFP-DDX6: 0.8 μL.
40 μM Tris pH7.4, 1 mM DDT, 10% glycerol: 2.5 μL.
40 μM Tris pH7.4, 1 mM DDT, 10% glycerol: 2.5 μL.
1M NaCl: 0.25 μL.

Accordingly, as needed, 1 μL p62 (10 μM) only, 2.5 μL poly-Ub (3 μM) only, or 1 μL p62 (10 μM) + 2.5 μL poly-Ub (3 μM) was used instead of buffer (40 μM Tris pH7.4, 1 mM DDT, 10% glycerol). Images were acquired on a 384-well plate with Leica DMi8 microscopy.

Basal phase separation buffer (BPSB): 0.3 μg/μl polyU, 5mM ATP (pH not adjusted), 10mM MgCl2, 50 mM NaCl2, 5% PEG 8000.

In vitro sedimentation assays

Purified recombinant proteins were centrifugated at 16,000 × g for 5 min to remove any potential protein aggregates, immediately prior to *in vitro* sedimentation experiments. The mixture (30 μL) of GFP-DDX6 protein (with control buffer), p62 + GFP-DDX6, or p62 + GFP-DDX6 + poly-Ub was subjected to *in vitro* phase separation at RT for 1 h in the buffer as described above. After 15-min centrifugation at 15,000 × g, the pellet and supernatant were separated. The pellet was washed once with the phase separation buffer, and resuspended in 30 μL phase separation buffer. The pellet and supernatant were probed by immunoblotting with indicated antibodies.

LDH cytotoxicity

CyQUANT LDH Cytotoxicity Assay, fluorescence kit (ThermoFisher Scientific, C20302) was used to measure cell toxicity. Lactate dehydrogenase (LDH) is a cytosolic enzyme, released into the media upon cell damage. The kit was used according to the manufacturer's instructions. Briefly, a cell culture-treated 96-well plate was seeded with 70,000–100,000 MPI cells/well resuspended in 100 μL complete RPMI supplemented with 1% GM-CSF containing X-63 media. Cells were incubated for 6–8 h for climatization and treated with 100 ng/mL LPS for 24 h or with 100 ng/mL LPS for 24h +20 μM nigericin for 2 h. 45 min before the end of the treatments, designated wells were lysed using 10 μL Lysis Buffer/well, to establish maximum LDH release. At the end of the treatments, 50 μL media/well was transferred to a fresh 96-well plate, topped with 50 μL Reagent Stock Solution and incubated in the dark at room temperature for 10 min. Post-incubation, 50 μL Stop Solution was added to each well, the plate was gently mixed by tapping, and bubbles were removed using a clean tip. The fluorescence was read using excitation/emission at 560/590 nm. The percentage of LDH released was calculated with respect to the maximum LDH detected in the lysed wells.

ELISA

The cell culture-treated 96-well plate was seeded with 100,000 MPI cells/well, resuspended in 180 μL complete RPMI supplemented with 1% GM-CSF containing X-63 media. Cells were incubated for 6–8 h for climatization. Subsequently, MPI cells were treated with 100 ng/mL LPS for 24 h or with 100 ng/mL LPS for 24h +20 μM nigericin for 2 h. Media were collected and subjected to enzyme-linked immunosorbent assay (ELISA). A clear, flat bottom 96-well plate was coated with 50 μL of purified anti-murine IL-1β antibody (3 μg/mL) (ThermoFisher Scientific, 14701285) diluted in 1 × PBS and incubated for 24 h in 4°C. Wells were blocked using 100 μL 2% BSA in 1 × PBS at room temperature for 1 h. Recombinant murine IL-1β protein (Peprotech, 211-11B) serial dilution was prepared in RPMI media for the standard curve as follows: 4000 pg/mL, 2000 pg/mL, 1000 pg/mL, 500 pg/mL, 250 pg/mL, 125 pg/mL, 62.5 pg/mL and RPMI only (blank). Samples were also diluted appropriately to ensure that their readings fit within the standard curve. Following blocking, 50 μL of diluted standards (in duplicates) and samples were added to the plate, and incubated for 2 h at room temperature. Subsequently, wells were incubated with 50 μL biotin conjugated anti-murine IL-1β antibody (2 μg/mL) (ThermoFisher Scientific, 13711285) diluted in 1 × PBS for 1 h at room temperature and with 50 μL Avidin-HRP (ThermoFisher Scientific, 18410094) diluted 1:500 in 1 × PBS for 30 min at room temperature. Finally, 50 μL Super AquaBlue ELISA substrate (ThermoFisher Scientific, 00420358) was added and incubated for 10 min at room temperature, prior to reading the absorption at 405 nm. In between each step, the wells were washed three times with PBS-Tween20 (1 × PBS, 0.05% Tween 20) and the plate was blotted dry on clean paper towels to remove residual wash buffer. A standard curve was drawn, and a four-parameter curve fit was used to determine the sample concentrations.

Gene Ontology (GO) analysis

Proteomic data were analyzed by the Gene Ontology (GO) resource (http://geneontology.org/) for pathway enrichment.

QUANTIFICATION AND STATISTICAL ANALYSIS

Particle analysis for cellular protein droplets

The sizes and numbers of p62 and other protein droplets in cells were measured with ImageJ (particle analysis). Single-channel images were exported, and the scale was set by drawing a line in parallel to the scale bar. Images were processed with the despeckle function to decrease the noise, and a threshold was set to highlight puncta. Puncta in each individual cell were selected by the

freehand drawing tool. The analyze-particle function was initiated for the sizes and numbers of the vesicles. Typically, 50 cells (n number) were analyzed. The analysis was conducted in a blinded manner by a researcher who was unaware of sample labeling and expected outcomes.

Statistical analysis

Statistical analysis was performed with Graphpad Prism v5. The Two-tailed unpaired T-tests were conducted for the comparison between two groups (***: $p < 0.001$; **: $p < 0.01$; *: $p < 0.05$; ns, not significant); one-way or two-way ANOVA tests were used for the comparison among multiple groups: One-way ANOVA for variables influenced by a single factor; two-way ANOVA for variables influence by two or more factors (***: $p < 0.0001$; **: $p < 0.01$; *: $p < 0.05$; ns: not significant). Data from at least three independent experiments were analyzed.